

# Measurement of aerosol and liquid droplet size distribution and validation of aerosol and droplet microphysical models



## Principal Investigator

**Prof. S. N. Tripathi**

Department of Civil Engineering  
I I T-Kanpur, Kanpur

## Co-Principal Investigator

**Dr. Tarun Gupta**

Department of Civil Engineering  
I I T-Kanpur, Kanpur

## Principal Collaborator

**Dr. B.K. Sapra**

Radiological Physics and Advisory Division  
BARC, Mumbai

## Co-Principal Collaborator

**Shri Sunil Ganju**

Reactor Safety Division  
BARC, Mumbai

## Sponsored by

Board of Research in Nuclear Sciences  
Project Ref. No: 2009/36/119-BRNS/3384  
Bhabha Atomic Research Centre  
Department of Atomic Energy  
Mumbai, India

---

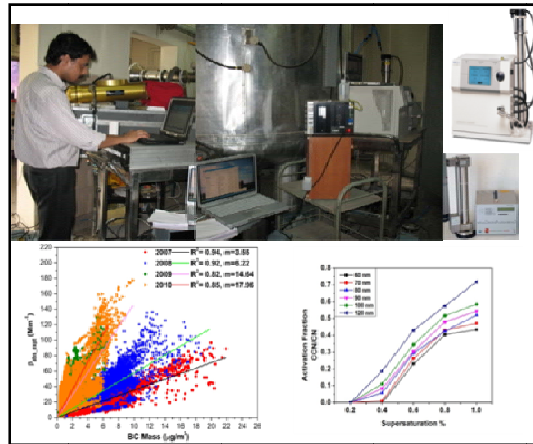
**Department of Civil Engineering  
I I T-Kanpur, Kanpur, Uttar Pradesh – 208016  
2013**

<b>1. Title of project</b>	<b>Measurement of aerosol and liquid droplet size distribution and validation of aerosol and droplet microphysical models</b>
<b>2. Principal Investigator</b>	<b>Dr. Sachchida Nand Tripathi</b>
<b>3. Co-Investigators</b>	<b>Dr. Tarun Gupta</b>
<b>4. Principle Collaborator</b>	<b>Dr. B.K. Sapra</b>
<b>5. Co-Principal Collaborator</b>	<b>Sh. Sunil Ganju</b>
<b>6. Research Scholar</b>	<b>Abhishek Chakraborty</b> <b>P.M. Shamjad</b>
<b>7. Research Associates /Technical staff</b>	<b>Anudbhav K. Dwivedi</b> <b>Harishankar</b>
<b>Project No</b>	<b>2009/36/119-BRNS/3384</b>
<b>Date of sanction</b>	<b>March 18, 2010</b>
<b>Period of project</b>	<b>Three Years</b>

## BRNS Project Report: 2009/36/119-BRNS/3384

# Measurement of aerosol and liquid droplet size distributions and Validation of aerosol and droplet microphysical models

November 2013



Principal Investigator (PI):  
Dr. S. N. Tripathi  
Prof., Department of Civil Engineering  
IIT Kanpur, Kanpur- 208016.

Co-PI:  
Dr. Tarun Gupta  
Assoc. Prof., Department of Civil Engineering  
IIT Kanpur, Kanpur- 208016.



Principal Collaborator (PC):  
Dr. B. K. Sapa,  
Radiological Physics and Advisory Division,  
B.A.R.C., Mumbai – 400 085.

Co-PC:  
Sh. Sunil Ganju,  
Reactor Safety Division  
B.A.R.C., Mumbai – 400 085.

Government of India  
Department of Atomic Energy  
BRNS Secretariat

Central Complex, 1st floor  
BARC, Mumbai 400 085

No. 2009/36/119-BRNS/ 3384

Date: 18/3/10

**Office Memorandum**

Sub: R/P entitled "Measurement of aerosol and liquid droplet size distributions and validation of aerosol and droplet microphysical models" under Dr. S.N. Tripathi, Indian Institute of Technology-Kanpur, Kanpur 208 016

On the recommendations of the Board of Research in Nuclear Sciences (BRNS), I am directed to convey the administrative approval and sanction of the President of India for the captioned project for three years beginning from financial year 2009-10 with a total grant of Rs.52,58,000/- as detailed below:

Item of expenditure	I year (2009-10)	II year (2010-11)	III year (2011-12)
@ Equipment	25,00,000	--	--
# Staff : RA (1)	2,16,000	2,16,000	2,16,000
\$ Technical Assistance	1,20,000	1,20,000	1,20,000
Consumable	2,00,000	1,00,000	1,00,000
Travel : PI	1,00,000	1,00,000	1,00,000
PC	1,00,000	1,00,000	1,00,000
Contingency	50,000	50,000	50,000
& Overheads	2,40,000	30,000	30,000
	35,26,000	7,16,000	7,16,000

@ (1) Condensation particle counter

# RA fellowship calculated @ Rs.18,000/- per month for three years (**revised**).

\$ Technical Assistance includes equipment hire charges, computer charges and charges for hiring services

& The remaining 7.5% towards overheads (Rs.3,00,000) shall be released only on meeting the requirements specified (**see Annex-B**).

2:

2. I am also directed to convey the sanction of the President of India to incur an expenditure of Rs.35,26,000/- towards grant for the year 2009-10.
3. The expenditure involved is debitable to :

Grant No.	:	05	-	Atomic Energy
Major Head	:	3401	-	Atomic Energy Research
Minor Head	:	00 004	-	Research & Development
Sub head	:	08 02	-	BRNS
Detailed Head	:	08 02 31	-	Grant-in-Aid
4. This issues with the concurrence of Scientific Secretary, BRNS and IFA.

Sd

(Dr. Debanik Roy)  
Programme Officer, BRNS

Pay and Accounts Officer  
Department of Atomic Energy  
CSM Marg  
Mumbai 400 001



No.2009/36/119-BRNS/ 3384

Date : 18/3/10

Copy forwarded to:

1. Director of Audit, Scientific Department, AEAP, OYC, CSM Marg, Mumbai - 400 001.
2. Joint Secretary (R&D), DAE, Anushakti Bhavan, CSM Marg, Mumbai-400 001.
3. Registrar, Indian Institute of Technology-Kanpur, Kanpur 208 016
4. \*\* Principal Investigator : Dr. S.N. Tripathi, Indian Institute of Technology-Kanpur, Kanpur 208 016

**A. First year grant is being released in full through Pay & Accounts Officer, Department of Atomic Energy, Anushakti Bhavan, CSM Marg, Mumbai-400 001 directly. You may await a DD/ MT, accordingly.**

- i) Receipt of this sanction letter and the DD/ MT for the amount sanctioned for the first financial year may please be acknowledged (Form-I).
- ii) THIS SANCTION IS FURTHER SUBJECT TO THE CONDITIONS STIPULATED IN ANNEX-A, ANNEX-B AND ANNEX-C (**ENCLOSED**), WHICH MAY BE GONE THROUGH CAREFULLY.

**B. Second year grant will be released after the PI submits the following documents to the Programme Officer (NRFC):**

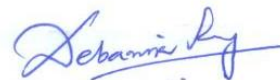
- a) Claim in Form-II (**enclosed**) quoting the reference of the sanction issued for the first year.
- b) Utilisation Certificate (UC) as on **31st March** of the preceding financial year in Form-III (**enclosed**) duly audited by the Internal Auditor of the University/ Institution or a Chartered Accountant.
- c) Statement of Accounts (SA) as on **31st March** of the preceding financial year in Form-IV (**enclosed**) duly audited by the Internal Auditor of the University/ Institution or a Chartered Accountant.
- d) Copy of appointment order and joining report of the staff appointed for the project along with minutes of the Selection Committee.
- e) An inventory of equipment in Form-V (**enclosed**).
- f) A One Page report on the progress of work during first year.

**C. Grant for the third year and subsequent years (if any), will be released only after the Principal Investigator (PI) fulfills the following requirement:**

- i) The Department will issue a fresh sanction for the third and subsequent years after receiving the recommendations of the BRNS after scrutiny of the Renewal Application in Form 4R.

Hence, **10 copies** of renewal request in the **Form 4R (enclosed)** and **3 copies** of detailed Progress Report must reach to **Dr. Vivekanand Kain, (MS, NRFC), Materials Science Division, BARC, Trombay, Mumbai-400 085** and one copy of **Form 4R** to **Dr. Debanik Roy, Programme Officer (NRFC), BRNS Secretariat, First Floor, Central Complex, BARC, Trombay, Mumbai-400 085** on or before **30th November** of the second or subsequent year of the project as the case may be.

- ii) If the progress is found to be satisfactory the renewal sanction for the year will be issued in the beginning of that financial year.
  - iii) On receipt of the renewal sanction, the PI shall claim the funds sanctioned by submitting the following documents to **Programme Officer (NRFC)**:
    - a) Claim in Form II (**enclosed**) quoting reference of the renewal sanction.
    - b) Utilisation Certificate (UC) as on **31st March** of the preceding financial year in Form-III (**enclosed**) duly audited by the Internal Auditor of the University/ Institution or a Chartered Accountant.
    - c) Statement of Accounts (SA) as on **31st March** of the preceding financial year in Form-IV (**enclosed**) duly audited by the Internal Auditor of the University/ Institution or a Chartered Accountant.
    - d) However, the final consolidated Statement of Accounts/ Utilization Certificate to be submitted at the end of the Terminal year shall be audited by a Chartered Accountant or the Statutory (Govt.) Auditor.
    - e) Copy of appointment order and joining report of the staff appointed for the project along with minutes of the Selection Committee.
    - f) An inventory of equipment in Form-V (**enclosed**).
    - g) Final consolidated Progress Report for settling the Terminal Grant.
5. AAO (Bills II), DAE, Anushakti Bhavan, CSM Marg, Mumbai - 400 001 – With a request that the amount granted for the first year of the project may be released immediately.
6. Member Secretary, NRFC : Dr. Vivekanand Kain, Materials Science Division, BARC, Trombay, Mumbai-400 085.
7. Member Secretary, TSC-4, NRFC : Dr. R.M. Tripathy, EAD, BARC, Mumbai 400 085
8. ✓ Principal Collaborator : Dr. B.K. Sapra, RP&AD, BARC, Mumbai 400 085 - You or your nominee may please be the DAE representative for selection of Research Fellow / Research Associate for the project.
9. Co-Principal Investigator : Dr. T. Gupta, Indian Institute of Technology-Kanpur, Kanpur 208 016
10. Sanction file.



(Dr. Debanik Roy)  
Programme Officer, BRNS

\*\* Note : Please quote the Sanction Number (**No.2009/36/119-BRNS**) in all your correspondence with BRNS.

# CONTENTS

Description	Page No.
<b>1. Introduction</b>	12
1.1 Review of earlier studies	13
1.2 BARC- Nuclear Aerosol Test Facility	17
1.3 Validation of computer codes	18
1.4 Current state of knowledge and motivation for project	19
<b>2. Experimental Facility and Instrumentation</b>	21
2.1 Scanning Mobility Particle Sizer	22
2.2 Aerodynamic Particle Sizer	24
2.3 Cloud Droplet Probe	25
2.4 Atomizer	28
2.5 Cloud Condensation Nuclei Counter	29
2.6 Nuclear Aerosol Test Facility	31
2.7 Experimental facility at IITK	33
<b>3. Containment Aerosol Behavior Code-NAUA</b>	35
3.1 General	36
3.2 Assumptions of the code	37
3.3 Code features	38
3.4 Code Validation	38
3.5 Mathematical framework of code	39
<b>4. Experiments on Harmonization of Particle Measurements</b>	
4.1 Intercomparison of Scanning Mobility Particle Sizers	41
4.1.1 Experimental details	42
4.1.2 Calibration of SMPSs using standard particles	45
4.1.3 Intercomparisons using Laboratory generated Particles	46
4.1.4 Comparisons in ambient conditions	50
4.2 Harmonization of particle concentration measurements	52
4.3 Case study: Application to Hygroscopic Growth of Black Carbon	54
4.3.1 Black Carbon Measurement	54
4.3.2 Experimental Setup	55
4.3.3 Calculation of Optical Parameters Using Mie Theory	56
4.3.4 Quantification of Hygroscopic Growth	56
4.3.5 Analysis of Optical Properties	58



---

4.3.6	Absorption Amplification	59
<b>5</b>	<b>NATF Experiments- Aerosol steam interaction</b>	<b>61</b>
5.1	Temperature profile in the test vessel in the presence of steam	61
5.2	Experimental protocol	63
5.3	Experimental Results	67
5.3.1	Aerosol size distributions	67
5.3.2	Measurement of Droplet Parameters	68
5.4	Comparisons with NAUA Code	71
<b>6</b>	<b>Condensation Activation of CsI aerosol</b>	<b>79</b>
6.1	Experimental set-up	80
6.2	Results and Discussions	82
<b>7</b>	<b>Conclusion</b>	<b>87</b>

---

## LIST OF FIGURES

Figure	Description	Page No.
1.1	Aerosol flow interactions in the reactor environment	13
2.1	Schematic diagram of a differential mobility analyzer	22
2.2	(a) Photograph of TSI APS 3320. (b) Schematic operation diagram of TSI APS 3320	25
2.3	Schematic diagram of Cloud Droplet Probe (CDP)	28
2.4	Photograph of TSI atomizer 3079	29
2.5	Supersaturation being generated in the CCNC column	30
2.6	Schematic diagram of Stream-wise thermal gradient CCN Counter	31
2.7	Schematic of Plasma Torch Aerosol Generation System	32
2.8	NATF test vessel and a typical set-up used for steam experiments	33
2.9	CDP sampling from test vessel	33
2.10	Aerosol Instrumentation in experiments	33
2.11	Experimental Facility at IITK	34
4.1	(a) Experimental set-up used at IITK for intercomparison of aerosol measurements. (b) Photographs of Scanning Mobility Particle Sizers used for intercomparisons	43
4.2	Calibration of the SMPSs using PSL particles 299nm and 499 nm.	46
4.3	CPC comparison for laboratory generated aerosols	47
4.4	SMPS comparison for laboratory generated test aerosols	48
4.5	CPC comparisons in low concentration ambient conditions	50

---

4.6	SMPS comparisons for ambient conditions	51
4.7	Harmonization of particle concentration measurements	52
4.8	Linear regression analysis between PASS-1 measured $\beta_{\text{abs}}$ and Aethalometer measured BC mass for four consecutive winter seasons at Kanpur	55
4.9	Schematic of Experimental Setup	56
4.10	Aerosol size distribution measured by Grimm SMPS and TSI SMPS for (a) in similar ambient condition, (b) when GRIMM was connected with a dryer and RH =76.5 %, (c) same as (b) but for RH = 74.2%, (d) same as (b) but for RH = 59.3%, and (e) same as (b) but for RH =66.3. $d_{\text{m,dry}}$ and $d_{\text{m,wet}}$ are dry and wet mode diameters, respectively and $g_{\text{exp}}$ is the growth factor	57
4.11	Comparison of $\beta_{\text{abs}}$ obtained from experiment and Mie Calculation	58
4.12	Comparison of $\beta_{\text{scat}}$ obtained from experiment and Mie Calculations	58
4.13	Absorption enhancements with respect to BC mass and shell thickness	59
5.1	Temperature profile (bulk) in test vessel during aerosol generation and steam feeding	62
5.2	A complete time series for experiment E1 (with Tin oxide)	66
5.3	A complete time series for experiment E3 (with Zinc oxide)	67
5.4	Steady state aerosol size distribution a) before and b) after steam for experiments E1, E2 and E3	68
5.5	MVD, LWC, DNC measured by CDP (for experiments E1-E3)	69
5.6	Comparison of particle depletion rates in E3& E2 with E5	70
5.7	LWC in presence of turbulence measured by CDP for E4	71
5.8	Experimental and code predicted number concentrations by SMPS and CPC for E3	72

---

---

5.9	Experimental and code predicted number concentrations by SMPS and CPC for E2	73
5.10	Experimental and code predicted number concentrations by SMPS and CPC for E1	73
5.11	Experimental and code predicted number concentrations for E5	74
5.12	Experimental and code predicted size distribution for E1	75
5.13	Experimental and code predicted LWC geometric mean diameter for E2	76
5.14	Experimental and code predicted LWC geometric mean diameter for E1	77
5.15	Code predictions of size distribution evolution for ambient conditions (E6)	78
6.1	Schematic showing the poly-disperse sampling using various instruments	80
6.2	Schematic showing the mono-disperse sampling using various instruments	80
6.3	Sampling manifold for chamber experiments	81
6.4	Schematic of aerosol generation and sampling in chamber	82
6.5	Time series of aerosol concentration inside the chamber (steady state)	82
6.6	Average aerosol size distributions (0.014–0.68 $\mu$ m) for 0.3 % CsI solution	83
6.7	Activation fraction of CsI aerosols (for mono-disperse conditions)	84
6.8	Activation fraction of CsI aerosols (a) Lower size particles (20-50 nm) (b) middle size particles (60- 120 nm) (c) higher size particles (150-310 nm).	85

---

## LIST OF TABLES

Table	Description	Page No.
4.1	Parameters of the SMPSs used in the study	44
4.2	Size segregated Relative Concentration Factor (RCF)	49
5.1	Operating conditions of plasma torch aerosol generator	63
5.2	Details of NATF aerosol-steam experiments	64
5.3	Time profiling for experiment E1	65
6.1	Comparison of activation diameter for CsI aerosols (experiment and theory)	86



## Chapter 1: Introduction

It is well understood that following a severe reactor accident, the radioactive materials are released into the primary heat transport system and subsequently into the reactor containment. These aerosols are composed of fission products, actinides and structural materials and their composition varies on the basis of source and generation mechanism. Since a high temperature gradient exists between core-plenum and further, between plenum-reactor coolant system (RCS); generation of aerosols from vapor/steam (homogeneous nucleation) and condensation on pre-existing aerosols (heterogeneous nucleation) becomes a major pathway for aerosol formation. These aerosols, released from the core in high concentrations, traverse the reactor coolant system and come out to the containment following a breach in the coolant system. The behavior of these aerosols in the coolant system becomes quite important as these act as a source term for the containment aerosols. The aerosol mass and number concentrations can reach near or more than  $1 \text{ g/m}^3$  and  $10^{13}/\text{m}^3$  in the containment, respectively.

The nature of aerosols in RCS and containment is affected by formation, growth, shape, deposition and resuspension of aerosol particles. The formation of aerosol particles can take place via mechanical comminution of materials or by nucleation and condensation of vapors. Entrainment of solids or liquid droplets in high flows, shock waves, high pressure melt ejection and droplet expulsion by gas bubbling through liquids are some of the mechanical processes which can produce aerosols. These processes produce particles in coarse range which generally don't remain airborne for a considerable amount of time. On the other hand, nucleation induced particle formation from supersaturated vapors is a more important source in reactor accident progression and consequence. High temperature conditions in the core vaporize radioactive materials which become supersaturated on reaching cooler regions near the core debris leading to the formation of aerosols in the ultrafine range.

The formed aerosols are distributed and mixed in the containment atmosphere by natural convective flows. Figure 1.1 represents typical aerosol flow interactions. It can be seen that decay heat from the core region leads to aerosol convective motion and droplet formation. Subsequently, various deposition and interaction mechanisms act on aerosols and decide their fate and life in the containment.

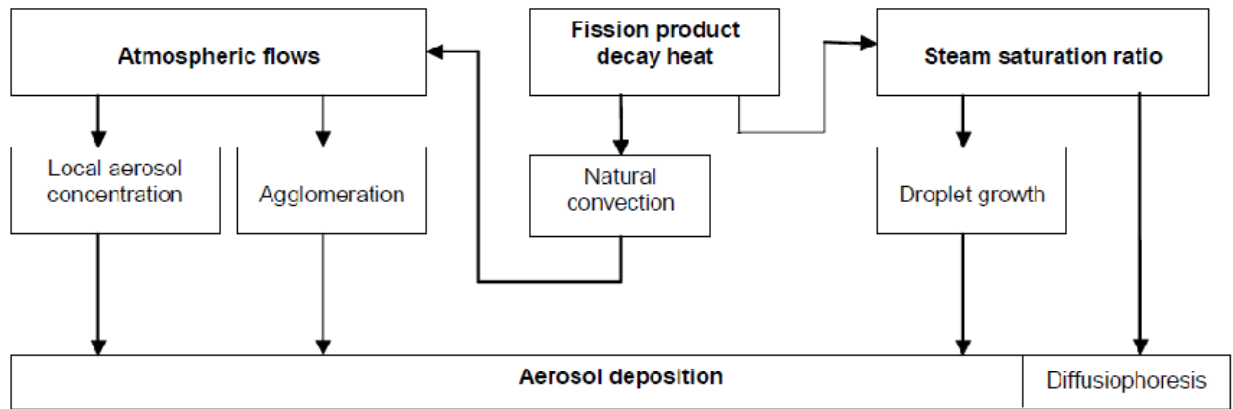


*Figure 1.1: Aerosol flow interactions in the reactor environment*

### 1.1 Review of earlier Studies:

Since TMI2 accident (1978), a lot of effort has been focused internationally on severe accident research and analysis involving separate-effect experiments, integral experiments and code developments. The theoretical studies have led to the development of computer codes coupling thermal-hydraulics with aerosol formation and dynamics mechanisms in different zones of the reactor. Key estimations such as fraction of aerosol activity released from the core, deposition mechanisms in RCS, characteristics of aerosols released into the containment and their fate etc. have been studied using these codes. The validity of these codes and further development of codes have been accelerated due to significant advancement of instrumentation technology and computational abilities. Large scale vital experiments have been performed under the umbrella of several experimental facilities and international co-ordination. Some of these programmers/experiments, their features and capabilities are discussed below.

## **PHÉBUS fission product programme**

The PHÉBUS FP programme intends to study Liquid Water Reactor (LWR) sever-accident phenomenon. The facility provides proto-type reactor conditions in which experiments have been performed for study of core degradation (involving melt pool formation), hydrogen production, FP release and transport, circuit and containment phenomena, and iodine chemistry. It has three components scaled down by roughly 1/5000 as compared with a French 900 MWe power plant. Studies have been performed in core region simulated by a 1-m long bundle of 20 irradiated fuel rods and a control rod, primary system components (where steam generator has been simulated by an inverted U tube) and in containment building simulated by a 10 m<sup>3</sup> tank including a sump, the atmosphere and painted wet and dry surfaces.

## **FALCON**

The small scale FALCON experiments were performed as preparation for PHÉBUS FP experiments at AEA Winfrith. The focus was on studying the influence of fission product chemistry on circuit transport and containment deposition, multi-component aerosol effects and vapor-aerosol interactions. Simulant fuel samples (CsI, CsOH, Te, SrO, BaO and MoO pellets clad in Zircaloy-4) with/without control rod alloy materials were heated by an induction furnace in a silica vessel resulting in bursting of fuel and control rod pellets, leading to continuous release of materials transported by carrier gas through the model circuit. Helium was used as the carrier gas having provision of mixing with low concentrations of steam and/or hydrogen. The injection of boric acid over the heated region was also made possible as an optional arrangement.

## **STORM**

The STORM series of experiments was performed at the European Commission's Joint Research Centre, Ispra (Italy) in the period 1996-97. Deposition experiments were performed in 63 mm diameter horizontal pipe of length 5000 mm with SnO<sub>2</sub> simulant aerosol carried by a steam-air-nitrogen mixture studying thermophoresis and eddy impaction. Nitrogen flow was used to disperse deposited fractions for re-suspension phase experiments. These two phases of experiments for STORM test 11 have been utilized for international standard problem ISP-40.

## **WAVE**

WAVE (Wide range Aerosol model Verification) facility experiments at JAERI were performed with the aim to investigate the cesium iodide (CsI) deposition onto the inner surface of a pipe under typical severe accident conditions. CsI placed at upstream pipe was electrically heated and generated CsI vapor or aerosol was carried to downstream pipe by nitrogen gas. Coupons placed in pipes were used to measure deposited mass.

## **DEMONA**

DEMONA tests were performed in 630 m<sup>3</sup> model containment made of reinforced concrete (simulating shape of German PWR containment) having several compartments. Nine large scale tests were carried out from 1983 to 1986 to investigate aerosol removal in a typical PWR containment under core melt down conditions. The validity of NAUA code was tested using the results of these experiments.

## **MARVIKEN-V**

The transport and deposition of aerosols and volatile species for a simulated LWR primary circuit was studied in large scale MARVIKEN-V tests during 1982-1985. Main components (reactor vessel, pressurizer, relief tank) were interconnected by pipes. Non-radioactive materials were used for fission product simulants (CsOH, CsI, Te) and core structure simulants (Ag, Mn). Evaporation-condensation type of aerosols (36-132 g/m<sup>3</sup>) was produced using plasma torches. Circuit geometry and test conditions were varied and the effect of temperature, superheated steam, condensing steam, and water were studied.

## **LACE**

The LACE tests were performed in a piping system connected to 852 m<sup>3</sup> volume (simulating an auxiliary building or a reactor containment building) to investigate aerosol behavior in high velocity gas flows and large volumes. The programme was sponsored by an international consortium in the latter half of the 1980's to understand and identify the aerosol issues for nuclear reactor accident research.

### **ACE-B: large scale combined effects experiment**

These experiments were performed at the Containment Systems Test Facility (CSTF), Hanford, USA. CSTF consisted of a large test vessel of volume 852 m<sup>3</sup>, aerosol generation facility and associated equipment. CsOH and MnO aerosol particles were fed in the test vessel in the first two phases. In addition, HI, in the first phase, and I<sub>2</sub>, in the second phase, were injected. Steam was continuously fed in order to keep the vessel wall at 100 °C for duration of about 4-5 days. The pH value of the sump was kept at 5.6 until the I<sub>2</sub> injection, during which it was simultaneously increased to 8.5. During the experiments, thermal-hydraulic parameters, temperatures, pressure, wall condensation rate, and pool water amount were measured together with deposition coupon samples. The aim of these experiments was to evaluate effectiveness of volatile iodine sinks (i.e., bulk aerosols, painted surfaces, steam condensation and water reservoirs).

### **VANAM**

Five large scale tests were performed in 626 m<sup>3</sup> Model Containment of the Battelle Institute in Frankfurt/Main (1988-1993). The containment had a multi-compartment geometry with locally different thermal hydraulic conditions. Local volume condensation and its effect on aerosol depletion, behavior of insoluble and hygroscopic aerosol materials in saturated and super-saturated steam-air atmospheres and Impact of a hydrogen deflagration on aerosol behavior (dry resuspension) was studied as a course of these experiments to generate experimental data for validation of coupled thermal hydraulic and aerosol codes.

### **KAEVER (including ISP-44)**

KAEVER project was carried out in Battelle Institute in Frankfurt/Main from 1993-1997. The objective of the experiments performed under this project was to study aerosol behavior under various thermal hydraulic conditions. These experiments used a horizontal cylindrical test facility (volume 10.6 m<sup>3</sup>) with provisions of thermal insulation and heating. Insoluble materials Ag and SnO<sub>2</sub> as well as hygroscopic materials such as CsI and CsOH were used as test aerosols. Both single-component aerosols as well as mixed-component aerosols were investigated.



## **AHMED**

AHMED facility constructed by VTT (Technical Research Centre of Finland) was used to investigate the discrepancies observed between results from model calculations and from large scale experiments. Hygroscopic NaOH, CsOH and CsI and inert Ag aerosol behaviour at different temperatures and relative humidity (RH) was studied in a well instrumented and controlled AHMED vessel of 1.81 m<sup>3</sup> total free volume. The uncertainties in thermal hydraulic part were aimed to be measured in experiments carried out in this vessel.

## **VICTORIA**

This facility (pressure vessel: height 4.6 m, diameter 3.14 m) is a scaled model of the ice condenser containment of Loviisa NPP with linear scale of 1:15 and volume scale of 1:3375. In the 1<sup>st</sup> phase programme (1990-1995), thermal-hydraulic behavior and hydrogen distribution were studied in severe accident conditions while a modified geometry was utilized in 1996-1997 for aerosol experiments. The objective of experiments carried out in this facility was to understand the radioactive hygroscopic and non-hygroscopic aerosol behavior in non-homogeneous multi-compartment containments and to validate containment aerosol models.

## **MCCI (ACE-C)**

Seven large-scale experiments on molten core concrete interactions (MCCIs) have been performed at Argonne National Laboratory as part of Advanced Containment Experiments (ACE) program. Aerosols released from experiments using four types of concrete (siliceous, limestone/common sand, serpentine, and limestone) and a range of metal oxidation for both BWR and PWR reactor core material have been collected and characterized. Release fractions were determined for UO<sub>2</sub>, Zr, fission products: BaO, SrO, La<sub>2</sub>O<sub>3</sub>, CeO<sub>2</sub>, MoU<sub>2</sub>, Te, Ru, and control materials: Ag, In and B<sub>4</sub>C. Release fractions of UO<sub>2</sub> and the fission products other than Te were small in all tests. However, release of control materials was significant.

### **1.2 BARC- Nuclear Aerosol Test Facility (NATF)**

As a part of strengthening the prediction capabilities of the aerosol codes used in the context of the safety assessment of Indian PHWR reactors, a Nuclear Aerosol Test Facility (NATF) has been built at the Bhabha Atomic Research Centre, India (Sapra et al., 2002). It is a medium scale

facility meant for carrying out aerosol behavior experiments under simulated accidental conditions and validating the aerosol behavior codes, mainly the NAUA MOD 5 code. The defined objectives of this facility are:

- (i) Investigation of spatial and temporal behavior of metallic or oxide aerosols in a test vessel under simulated post-accident conditions of the containment atmosphere characterized by pressure, temperature and humidity.
- (ii) Study of aerosol scrubbing phenomenon in a water pool simulating the suppression pool of nuclear power plants.
- (iii) Validation of existing computer codes for aerosol behavior studies in the containment of nuclear power plants.
- (iv) Estimation of source term for atmospheric dispersion models.

Based on the above objectives series of experimental studies were carried out from the point of view of understanding the physical aerosol dynamics and their consequent behavior. These physical mechanisms form the core of the aerosol behavior computer codes. In a broad sense, the aerosol systems of nuclear interest may be classified as (i) dry solid particles (ii) particles in the presence of steam, and (iii) volatile and semi-condensable vapors. In the first phase, validation of the dry aerosol behavior through controlled experiments was carried out in quiescent and turbulent flow conditions. These focused on examining the spatio-temporal variations of the airborne concentrations and the evolution of the size distribution and comparisons with the code predictions.

### **1.3 Validation of computer codes**

All above facilities provided extensive data facilitating the growth of knowledge related to reactor accident research and also helped code developers to develop and validate codes intended for reactor programmes. The analysis of the experimental results was carried out using various computer codes which are basically categorized into three types:

- **Separate phenomena codes:** These codes attempt to model phenomenon on the basis of experimental data availability. These act as benchmarks for integrated codes and are used in severe accident research.
- **Integrated PSA codes:** These codes attempt to address set of phenomenon that occurs during specific severe accident sequence. They incorporate the thermal-hydraulics, chemical and fission product models into a single code for the core, primary and secondary coolant systems, and the containment building.
- **Simple parametric codes and computational tools:** These codes are intended for specific PSA applications in which the assessment of uncertainties on accident progression pathways requires extensive repetitive calculations. These are based on simple parametric models which interpolate between fixed points for which calculations with a more detailed code have been performed to determine the values of the parameters.

#### **1.4 Current state of knowledge and motivation for this project**

Most of the above discussed facilities and experiments were carried out in a way to measure and quantify aerosols in a collective sense. Gross samplers, deposition coupons, impactors were used for physical measurements; while chemical behavior was utilized for understanding chemical properties of aerosols. However, the last two decades has seen a tremendous growth in aerosol instrumentation with capabilities to measure number concentration as well with faster temporal resolution. In addition, instruments capable of measuring droplet properties have become commercially available in the recent past, which can provide key information on the droplet phase of aerosols.

Beyond any doubt, small scale and large scale experiments performed worldwide have helped to bridge the knowledge gap required for understanding the key processes and phenomenon related to aerosol research in context of severe reactor accident. The development of several computer codes simultaneously has also utilized the multiplicative growth in computational abilities. It is important to supplement the severe accident aerosol research programme by carrying out the next level of experiments utilizing the newer age of aerosol instrumentation and techniques. Also, the applicability of the experiments carried out in the worldwide facilities (intended for

individual country reactor programs) is questionable for its relevance towards the Indian PHWR program.

As far as studies at BARC are concerned, NATF 1<sup>st</sup> phase experiments have been focused on dry aerosol experiments and the results have been implemented for testing of codes. In order to strengthen aerosol research program for IPHWR, several experiments (such as piping deposition, thermophoretic experiments, dry and wet aerosol behavior in containment) have been conducted in the recent past. Following these experiments, next phase of the NATF research aims at conducting experiments on aerosol steam interaction. In this direction, BRNS project with IITK was undertaken with the following objectives.

1. Measurement of aerosol & liquid particle size distribution
2. Cloud condensation nuclei measurement
3. Estimation of liquid water content
4. Particle optical properties
5. Validation of NAUA Mod 5 under steam environment

In order to achieve the above mentioned objectives, experiments have been carried out in three stages. In the first phase harmonization of aerosol instruments available with BARC and IITK labs has been carried out to arrive at a correlation factor. These factors were used to understand the optical properties of black carbon aerosols as a case study. In the next phase, several experiments were carried out in NATF chamber to study the aerosol steam interactions. Aerosol and droplet characteristics were measured for tin and zinc oxide aerosols. The results of these experiments were compared with the Containment aerosol code NAUA available at BARC. In the third and last phase, hygroscopic behavior experiment for CsI aerosols was performed.

This report discusses work carried out pertaining to the above discussed phases. In the following chapter (Chapter 2), instrumentation and facility description have been provided. Chapter 3 discusses various nuclear aerosol codes and NAUA code which was used for comparing the experimental observations. Chapter 4 presents experiments and conclusions related to harmonization of the instruments used in the project. Chapter 5 and 6 elaborates experimental methodology, results and experiment-code comparison of aerosol steam interaction and CsI activation, respectively. The report concludes in chapter 7 stating results of various phases of the project.

## Chapter 2: Experimental Facility and Instrumentation

The experiments carried out under this project had multi-fold objectives making it necessary to utilize a wide range of instruments to deduce meaningful results. Additional complexity in instrumentation and measurement arises due to the fact that, no single aerosol instrument can cover an entire size range from nano- to coarse range particles. Also in relatively high humidity conditions, most instruments used for aerosol number concentration and size distribution measurements become non-functional. Hence a wide set of aerosol instrumentation available with BARC and IITK laboratory was utilized during these experiments. Aerosol number concentration has been measured using GRIMM condensation particle counter (CPC) while TSI scanning mobility particle sizer (SMPS) and TSI aerodynamic particle sizer (APS) have been used for size distribution measurements. This selection covered all aerosol particles ( $> 4.5$  nm) in terms of number concentration while size range of 10 nm- 20  $\mu$ m could be covered for size distribution. However these instruments cannot be used for measurements, when relative humidity (RH) of air (presence of droplets) becomes high (near 100 %) with high temperature aerosol conditions ( $> 45$  ° C). For such conditions, cloud droplet probe (CDP) available with IITK has been used which is capable of measuring droplet properties in terms of concentration, mean diameters and liquid water content.

For controlled experiments aimed at studying the hygroscopic behavior of cesium iodide aerosols, steady aerosol generation and different super-saturation conditions sustainable for a desired amount of time is required. Cloud condensation nuclei counter (CCNC) of IITK has been implemented for these controlled chamber experiments. TSI atomizer has been used for the purpose of producing steady aerosols which consequently were used for sustaining steady conditions in the chamber. Although a mention of NATF test vessel has been made previously, it



is worthwhile to discuss this facility (of BARC) under this section. A brief summary of the facility parameters, aerosol generation system, characterization module and controls has been presented in the subsequent sections.

## 2.1 Scanning Mobility Particle Sizer (SMPS)

SMPS includes a differential mobility analyzer (DMA) and a Condensation Particle Counter (CPC) which acts as an aerosol detector. It can measure size distributions in the diameter range of 2.5-1100 nm. Different parts of the SMPS are the DMA classifier, neutralizer, sheath air flow, central rod (voltage) and condensation particle counter. (See figure 2.1)

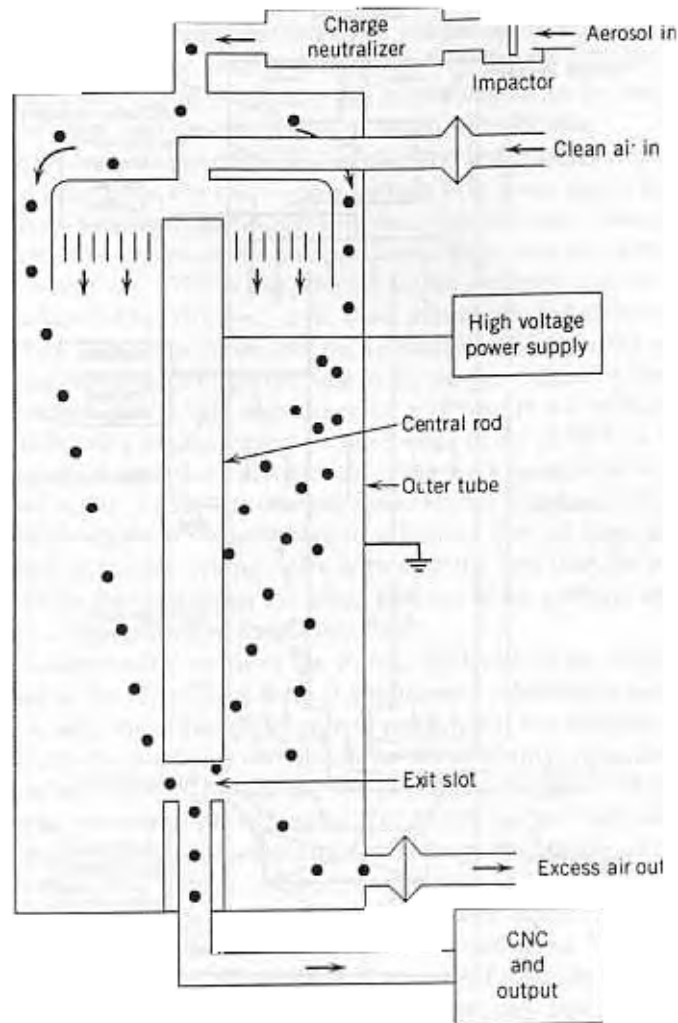


**Figure 2.1:** Schematic diagram of a differential mobility analyzer

The DMA Classifier consists of two cylindrical electrodes made of stainless steel insulated from each other by a plastic spacer at the bottom. The lower spacer allows enough high voltage leakage to prevent static charge build up near the exit slit. This results in a better particle transport for even the smallest particle. The central electrode is coaxially arranged to the outer electrode which is connected to a positive/negative high voltage supply. The neutralizer is an alpha or beta source (Am-241) or (Kr-85) used as a bipolar charger to get a well-defined charge distribution on the particles. Nearly all particles from 3-300 nm receive a single positive, negative or zero charge (Boltzmann distribution) while multiple-charging corrections are applied for other sizes. The particles then enter the electrostatic column and the applied high voltage can classify the aerosol according to the electrical mobility of the particles.

The Sheath Air Flow supplies filtered particle free- air, which enters through a round chamber at the top of the classifier. This air flows axially downward to the classifying section. The polydisperse sample airflow enters the classifier through an inlet pipe from top and flows in an axial direction between two narrow concentric cylinders ensuring a homogeneous distribution and a concentric flow. The Central Rod (voltage) is the parameter that controls the particle size generated by the classifier. The rod voltage ranges from 0-10,000 volts. The outer cylinder can be charged to a defined negative/positive potential. So, positively/negatively charged particles move towards the outer wall and the neutral particles go straight along the DMA. Only a narrow group of electrical mobility sized particles move towards the central rod for a given applied voltage which are then detected and counted by a Condensation particle counter (CPC).

CPCs are often used as detectors with other instruments such as electrical mobility classifiers to measure the total aerosol number concentrations larger than a minimum detectable size. Particles are grown by condensation in CPCs until they are sufficiently large to be detected optically (diameter growth factor - 100 to 1000). CPCs provide an extraordinarily sensitive means for detecting small sizes ( $\approx 2.5$  nm). A variety of substances have been used as the condensing vapor, but water and n-butyl alcohol is currently used most often. Because the super saturation of the condensing vapor is very high, the response of CPCs is typically insensitive to the composition of the measured particles. It is advantageous to use a high molecular weight working fluid with instruments of this type to ensure that sufficient cooling (and therefore super

saturation of the vapor) occurs before vapor is depleted by condensation on the cool walls. The working fluid should also have a vapor pressure that is high enough to cause particles to grow to about 10 $\mu$ m during the  $\approx$ 0.3 s flow time through the condenser but low enough to ensure that the vapor is a small fraction of the total gas flow. As N-butyl alcohol (heated to 35°C) meets these requirements, it is used in the CPC model used in the present study. In CPC model GRIMM 5.403, the larger sized particle droplets cross a laser beam where each droplet scatters light onto a photo-diode. These signals are continuously counted, stored and converted to particles/cm<sup>3</sup> which can be displayed on the screen. The sampling flow rate of this model is 0.3 liters per minute.

In this work, scanning mobility particle sizer (TSI 3696) has been used for aerosol number size distribution measurements. GRIMM CPC (5.403C) has been used for measuring integral concentration greater than 4.5 nm and up to 10<sup>8</sup> particles/cm<sup>3</sup>. For size distribution measurement, SMPS measured aerosol diameters from approximately 14 nm to 800 nm.

## **2.2 Aerodynamic Particle Sizer (APS)**

The APS measures size distribution of aerosols having aerodynamic diameter between 0.3-20  $\mu$ m. Aerodynamic diameter is the most important size parameter because it determines the airborne behavior of the particle. APS measures aerodynamic size measurements in real time using low particle accelerations. The TSI APS 3320 (Figure 2.2 (a)) is a time-of-flight spectrometer that measures the velocity of particles in an accelerating air flow through a nozzle. In the instrument, particles are confined to the centerline of an accelerating flow by sheath air. They then pass through two broadly focused laser beams, scattering light (See Figure 2.2 (b)). Side-scattered light is collected by an elliptical mirror that focuses the collected light onto a solid-state photo-detector, which converts the light pulses to electrical pulses. By electronically controlling timing between the peaks of the pulses, the velocity can be calculated for each individual particle. Velocity information is stored in 1024 time-of-flight bins. Using polystyrene latex (PSL) sphere calibrations, which are stored in non-volatile memory, the APS Model 3320 converts each time-of-flight measurement to an aerodynamic particle diameter. For convenience, this particle size is binned into 52 channels (on a logarithmic scale). The particle range spanned by the APS is from 0.5 to 20  $\mu$ m in both aerodynamic size and light-scattering signal. Particles

are also detected in the 0.3 to 0.5  $\mu\text{m}$  range using light -scattering alone, and are binned together in one channel. The APS is also capable of storing correlated light-scattering-signal data and time-of-flight data.



*Figure 2.2 (a): Photograph of TSI APS 3320*

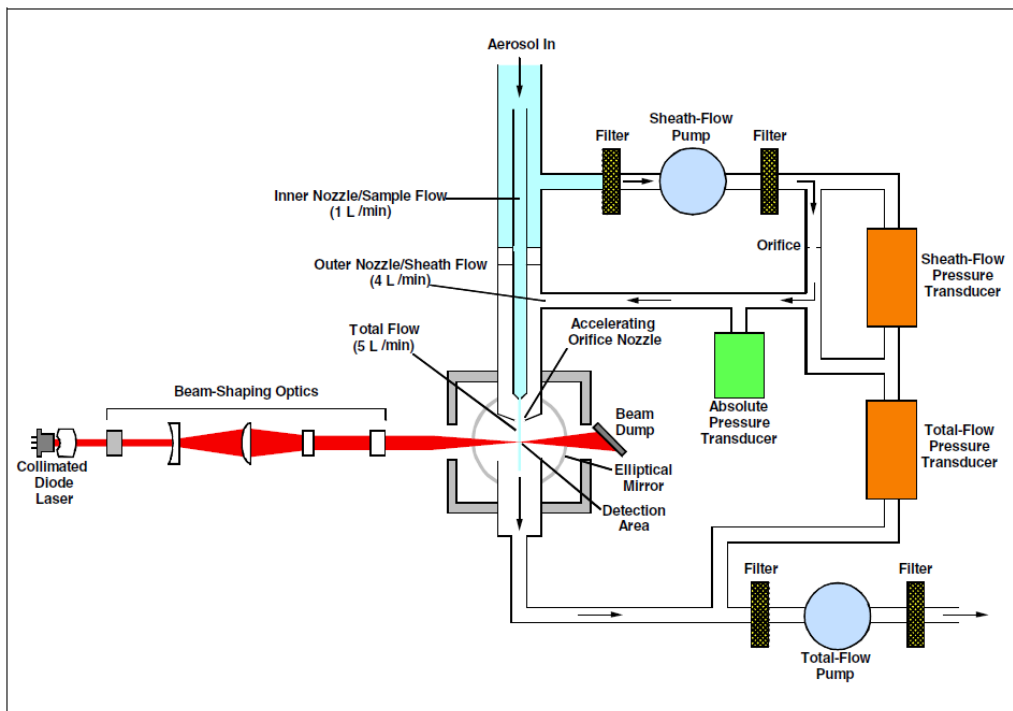


*Figure 2.2 (b): Schematic operation diagram of TSI APS 3320*

### 2.3 Cloud droplet probe (CDP)

The Cloud Droplet Probe (CDP) is designed to measure cloud droplet size distribution from 3 to 50  $\mu\text{m}$  size range. It also measures average drop diameter, mass-weighted diameter, mode distributed diameter and liquid water content (LWC). The miniaturized and streamlined housing

allows its usage in a variety of ground-based or airborne applications. It contains the forward scattering optical system, which includes a laser heating circuit, photo detectors, and analog signal-conditioning. The signals are transmitted via a robust differential driver/receiver interface to the CDP Electronic Module, or CDPE (Jariwala et al., 2009; Banerjee et al., 2012; Singh et al., 2011).

The operating principle of CDP is based on the concept that the amount of light scattered by a particle is proportional to its size. In addition to this, the droplets counted and sized in a selected time period must be converted to a number concentration and LWC. This requires a definition of the sample volume. This is defined by the sensitive area of the laser beam, the air speed, and the sample time. The sensitive area of the laser beam is defined by a combined optical and electronic technique that selects a depth of field (DOF) which is a certain length along the beam, and an Effective Beam Diameter (EBD) which is a portion of the beam width. Optics transmit a magnified image of the scattered light to photo-detectors, but one of the detectors has a circular mask on its surface that prohibits it from receiving light from particles that are about 1.5 mm either side of the focal plane. The electronics compare the pulse amplitudes from the masked detector, with that of the detector seeing all of the light scattered in the forward direction (signal detector). Particles that can be seen by the masked detector are rejected, since they are outside the DOF. The laser beam is not uniformly intense over its cross section and hence the entire beam diameter cannot be utilized. Otherwise, particles passing near beam edges would be undersized. The EBD is a fraction of the physical beam diameter, and is defined electronically by measuring the transit time of all particles that are accepted within the DOF, maintaining an average of their transit times, then rejecting individual particles whose transit times are less than the average (signifying that they must have gone through near the edge).

Particle concentration is defined as the number of particles per unit volume and is also the 0<sup>th</sup> moment of the size distribution.

$$C_T = \sum_{i=1}^m \frac{n_i}{SV} \quad (1)$$

where,

$C_T$  = total concentration

$n_i$  = number of particles accumulated in channel  $i$

$m$  = total number of size channels

$SV$  = sample volume =  $DOF \times EBD \times V \times t$ , where  $V$  is the airspeed and  $t$  is the sample period.

$EBD$  = (Beam Diameter)  $\times$  (Gated Strobes) / (Total Strobes)

The mean diameter is the weighted average of all the particle sizes, also known as the 1<sup>st</sup> moment of the size distribution, and is calculated by

$$D = \sum_{i=1}^m \frac{C_i d_i}{C_T} \quad (2)$$

where  $C_i$  is the concentration of particles with size  $d_i$ .

The liquid water content,  $W$ , is calculated from the measured size spectra using summation of the individual particle masses per unit sample volume, i.e.

$$W = \pi * \rho_w * \sum_{i=1}^m \frac{C_i d_i^3}{6} \quad (3)$$

where,  $\rho_w$  = density of water.

The schematic diagram of the CDP is shown in Figure 2.3. As particles pass through the laser beam, light is scattered in all directions. The cone of photons that is forward scattered in the 4° to 12° range is collected and directed onto a 33/66% optical beam splitter, and then a pair of photo detectors. The photo detectors convert the photon pulses into the electrical pulses. One photo detector sees 33% of the collected light and other sees 66% of the light collected from particles that pass through the laser beam if, and only if, the scattered light is collected and focused through the optical mask, is called the Depth of Field (DOF). The outputs from these two detectors are referred to as Sizer (33%) and Qualifier (66%). The intensity of the scattered light will depend upon the size, composition, shape of the particle, and the intensity and wavelength of the incident laser light. The amount of light collected will depend upon the distance of particle from the collecting optics when it passes through the beam.

For accurate sizing, the CDP must accept and size only particles that pass through a uniform power region of the laser beam: creating the need for the “qualified” particle. The voltage pulse from the sizing detector is compared with the voltage pulse from the qualifying detector, and a digital flag is raised if the masked detector’s output exceeds that of the signal to be sized. If DOF

flag is not raised, then those particles are DOF-rejected. Once the photon pulse has been converted, amplified, and DOF qualified, the analog voltage value is digitized and categorized. The peak digital value is then categorized onto one of 10, 20, 30 or 40 bins. The CDPE Version-2 (which includes FPGA (Field Programmable Gate Array) technology) enables a second histogram to be generated. This histogram contains information on the time between particle events allowing the actual distance between particles to be determined.

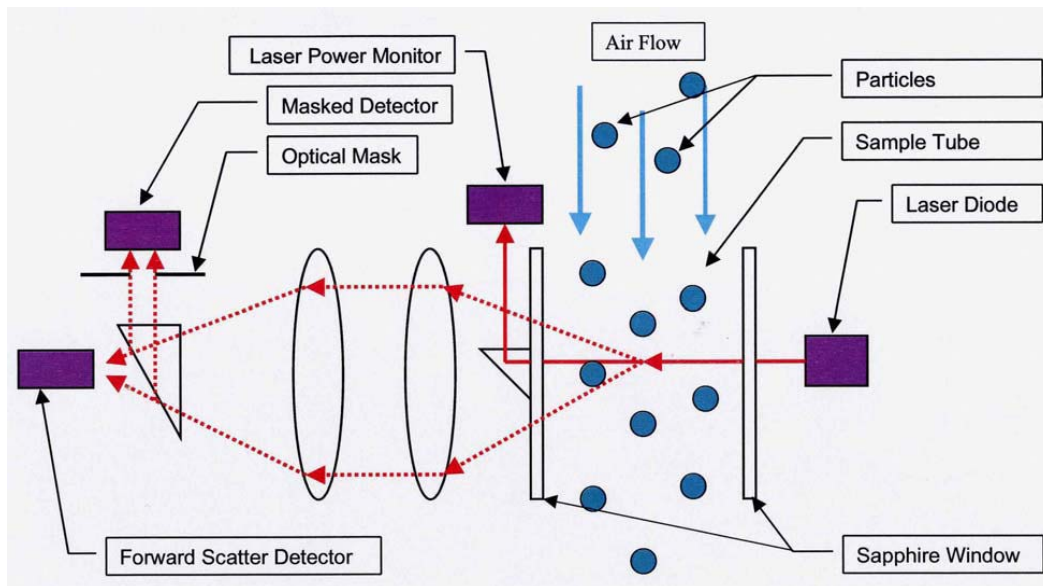


**Figure 2.3:** Schematic diagram of Cloud Droplet Probe (CDP)

## 2.4 Atomizer

TSI 3079 atomizer has been used in this work for inter-comparison experiments and CsI aerosols hygroscopic behavior study. It uses a compressed air nebulizer to produce polydisperse aerosols. The compressed air, after passing through high efficiency filters expands through the nozzle producing a high velocity jet. This high velocity air flow breaks the solution (drawn from atomizer vessel due to negative pressure) into droplets and suspends these droplets in air flow. An impactor is used to cut-off higher sizes and controlled fine aerosols then can be used for experiments. The aerosol concentration can be varied using a flow rate which can be changed from 1 to 4.2 Lmin<sup>-1</sup>. Figure 2.4 shows a picture of atomizer used for this study.



*Figure 2.4: Photograph of TSI atomizer 3079*

## **2.5 Cloud Condensation Nuclei Counter (CCNC)**

The DMT (Droplet measurement Technologies) make CCN counter is a cylindrical Continuous-Flow Stream-wise Thermal-Gradient Diffusion Chamber. It measures aerosol particles that have the ability to form into cloud droplets at specific supersaturation (%SS).

CCNC operates on the principle that diffusion of heat in air is slower than diffusion of water vapor (Roberts and Nenes, 2005). Inside the column, a thermodynamically unstable, supersaturated water vapor condition is created. A constant centerline supersaturation develops from the difference between thermal and water vapor diffusivity. Water vapor diffuses from the warm, wet column walls toward the centerline at a faster rate than the heat. Figure 2.5 shows point C along the centerline where the diffusing heat originated higher on the column (red-line, point A) than the diffusing mass (blue line, point B). Assuming the water vapor is saturated at the column wall at all points and the temperature is greater at point B than at point A, the water vapor partial pressure is also greater at point B than at point A. The actual partial pressure of water vapor at point C is equal to the partial pressure of water vapor at point B. The temperature at point C is lower than at point B, however, which means that there is more water vapor (corresponding to the saturation vapor pressure at point B) than thermodynamically allowed. The supersaturated water vapor condenses on the cloud condensation nuclei in the sample air to form droplets, which are further counted by OPC using scattering technology.



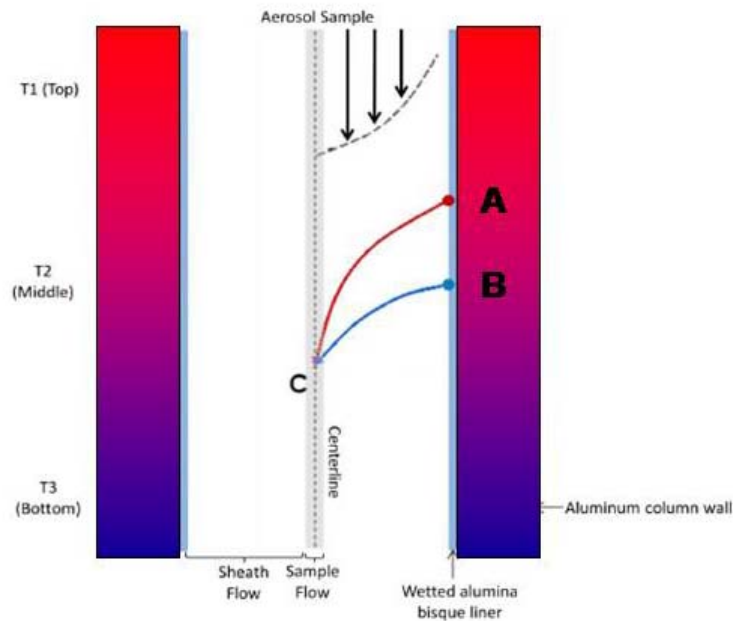


**Figure 2.5:** *Supersaturation being generated in the CCNC column*

The inlet flow is split into two parts: sample flow and sheath flow with a flow ratio of 1:10 (see Figure 2.6). The sample flow is directed to the center of the column whereas the sheath flow is filtered and humidified prior to its entry into the chamber resulting in a blanket of sheath air over the sample flow. Both the flows travel through the column exposed to constant supersaturation. Aerosol particles whose critical supersaturation is below the instrument supersaturation will activate into droplets. An optical particle counter counts and sizes the droplets at the outlet of the column, using a 50mW, 658 nm laser diode. All scattered light between 35° to 145° is collected and detected with a photodiode. A multichannel analyzer bins detect and segregate droplets into 20 size classes (0.75 to 10  $\mu\text{m}$ ).

A recent study has shown that at higher CCN concentrations, the supersaturation generated in the column gets depleted by the condensation of water vapor on the growing CCN. So, it is advisable to account for supersaturation depletion effects for unambiguous measurements of CCN activity and droplet activation kinetics (Lathem and Nenes, 2011; Patidar et al., 2012; Srivastava et al., 2013).

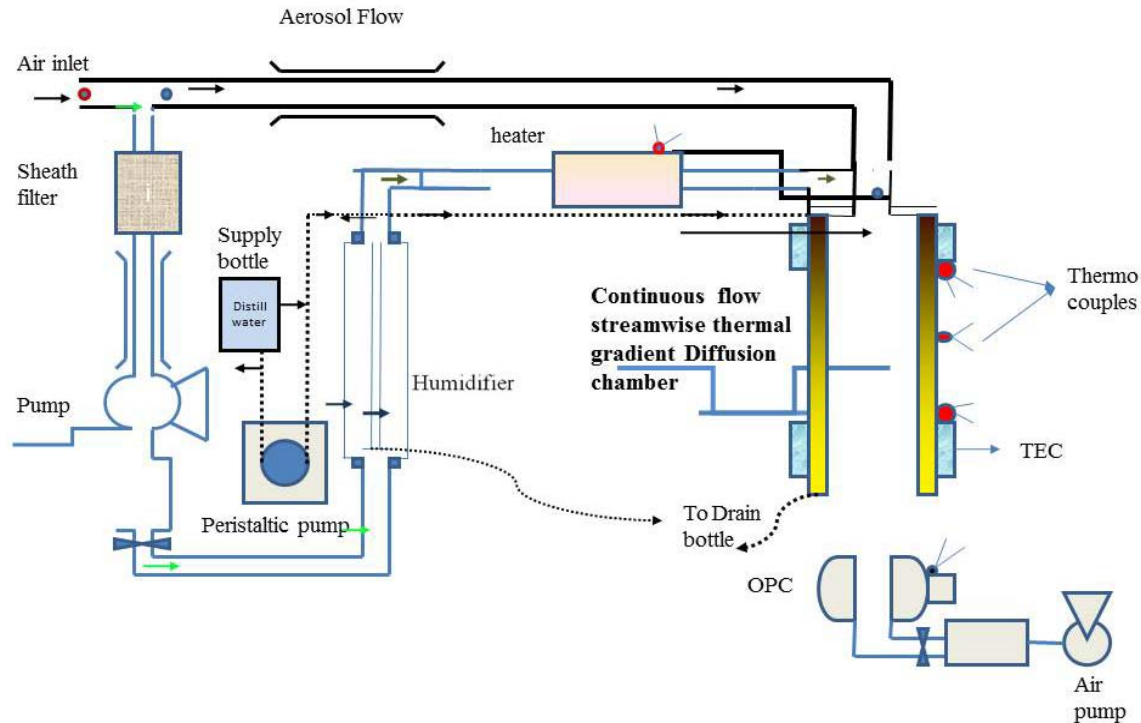


*Figure 2.6: Schematic diagram of Stream-wise thermal gradient CCN Counter*

## 2.6 Nuclear Aerosol Test Facility (NATF)

This facility of BARC was used for carrying out the pivotal experiments (i.e. related to aerosol-steam interactions) under this project. The main components of this facility are aerosol generator, test vessel and measurement/control systems.

A Plasma Torch based Aerosol Generator (PTAG) system, commonly used in several test facility studies the world over, is used for generating test aerosols in this facility. The main reason for using PTAG is its capability of producing condensation and evaporation type, continuous high intensity aerosols of metallic and ceramic powder. In accident simulation analysis, this is best suited and can generate aerosols in the concentration range of few  $\text{g}/\text{m}^3$ . Figure 2.7 shows the schematic of the PTAG along with its components. The details of the design and characterization of the system have been discussed in detail by Shreekumar et al. (1996).

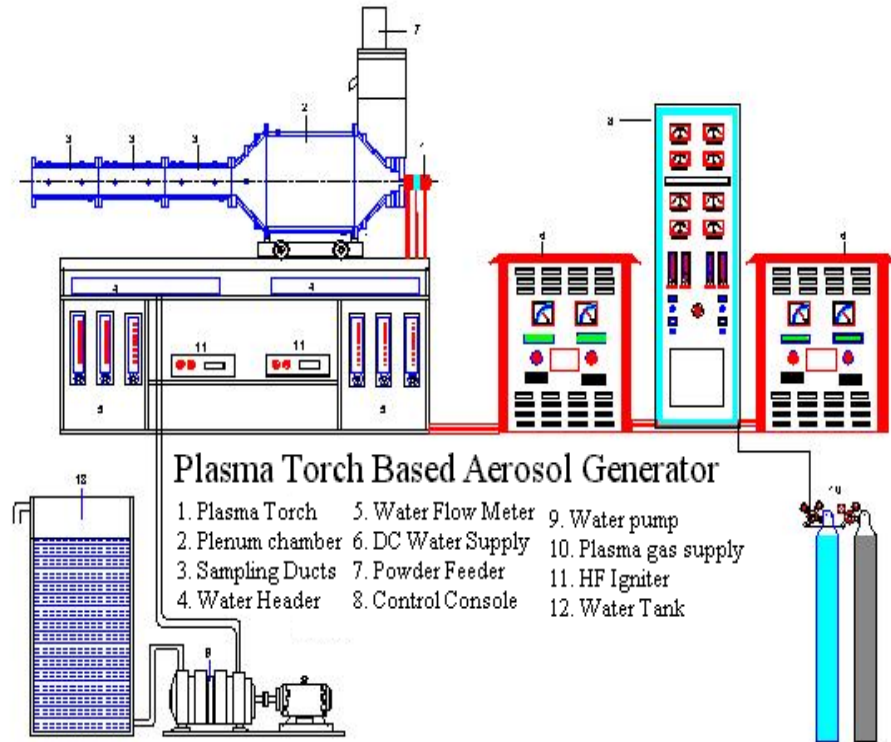


**Figure 2.7:** Schematic of Plasma Torch Aerosol Generation System

Aerosols generated by the PTAG are transported through the plenum chamber to the test vessel (Figure 2.8). This is a stainless steel cylindrical vessel with conical end fittings, having an air space volume of about 10 m<sup>3</sup>. The vessel is equipped with one pressure gauge and 28 temperature sensors. The temperatures of the bulk gas and the wall of the vessel are monitored at different levels. The sensors are connected on-line to a multi-channel scanner device coupled to a PC. The vessel is fitted with probes for sampling aerosols, which are stainless steel tubes having 3/8<sup>th</sup> inch diameter with lengths varying up to 1 m. Provisions have been made for injecting aerosols and steam into the vessel. Steam line (1" dia) is provided to introduce the steam into the vessel at a pressure of 2 kg/cm<sup>2</sup>. A drain line is connected at the bottom of the vessel to drain out the condensed water during wet experiments with steam. A HEPA filtration unit is attached at the top of the vessel to clean the aerosol bearing air and discharge it into the open atmosphere. A detailed description of the facility is given in Mayya et al (2008).



**Figure 2.8:** NATF test vessel and a typical set-up used for steam experiments



**Fig 2.9** CDP sampling from test vessel



**Fig 2.10** Aerosol Instrumentation in experiments

## 2.7 Experimental Facility at IITK

This facility of IITK is used for carrying out the laboratory generated aerosol experiments. The main components of this facility are aerosol generator, Plexiglas chamber and CCNc, SMPS and CPC. The plexiglas chamber having a volume of 40 liters was equipped with a small fan to homogenize the aerosols and four sampling ports. The lower port of the chamber was connected to a commercial nebulizer (TSI aerosol generator 3079) which was operated at  $0.9 \text{ Lmin}^{-1}$  for all experiments. One of the upper ports was used with a flow divider and connected to CCNC, SMPS (classifier 3080 with CPC 3775) and CPC 3776. All three instruments were operated at

their default flow setting i.e. at aerosol sampling flow rate of 0.3 liters per minute. Another port was used for HEPA filter to maintain a constant flow rate of 0.9 Lmin<sup>-1</sup>. Artificial aerosol was generated by a constant output atomizer (TSI; 3079) using aqueous solutions of inorganic salts. The nebulized aerosols were conditioned using silica based diffusion dryer to reduce the RH up to 20% before entering into the chamber. Electrically non-conducting flexible tubes were used to minimize the losses due to aerosol charges. All the connections have same length and orientation to minimize the particle loss. The tube length after the flow divider was kept 0.5 m for all instruments.



*Fig 2.11 Experimental Facility at IITK*



## Chapter 3: Containment Aerosol Behavior Code- NAUA

In a coupled thermal-hydraulic aerosol model with multi-compartment capability, aerosols can be considered, in a first-order approximation, as tracer substances that are transported between the compartments by the advective flow velocities calculated in the thermal hydraulic model part. Agglomeration acts as a mass transfer mechanism between aerosol size classes, and deposition acts like a sink term to the airborne aerosol concentrations. The aerosols may be represented by a certain number of size classes. Advective aerosol transport over vertical flow paths interferes with the sedimentation velocity of the particles. Since this velocity depends upon the particle size, the effective aerosol transport velocity can be considerably higher than the gas velocity, especially for larger particles. Steam condensation on aerosols has a major impact on the overall deposition rate. In order to achieve a consistent model for steam condensation on aerosols, the following effects must be taken into account:

- steam and gas sources and sinks, inter-compartment flows;
- heat transfer rates to walls;
- steam condensation on walls;
- evaporation;
- gas pressure and temperature;
- Steam transfer to aerosol particles, and removal of condensation heat.

By means of a mass and energy balance of the atmosphere in a computational zone, a thermodynamic state can be determined which is generally different from thermal equilibrium or saturation.

If the result is super-saturated, the amount of steam that exceeds the saturation concentration can be considered as fog formation mass because equilibrium conditions are achieved within seconds, as determined by Mason's rate equation. Particle growth in super-saturated steam is affected by the Kelvin effect resulting from the surface tension of the aerosol droplets and the corresponding equilibrium steam pressure on the surface of the droplets. Due to this effect, a critical droplet size exists, with droplets of smaller size being unable to grow under given supersaturation conditions.

A major part of the aerosols from a core meltdown accident are hygroscopic, especially due to CsI and CsOH components. Steam is condensed on hygroscopic aerosols even under superheated atmospheric conditions, and release of hygroscopic particles can increase the superheating. Modeling steam condensation on hygroscopic aerosols requires a consistent simultaneous treatment of heat and mass balances, including the aerosol water–steam exchange in each computational zone. This is much more complicated than modeling steam condensation on non-hygroscopic aerosols, the latter being a pure thermodynamic calculation without any feedback from aerosol behavior.

Two more coupling effects between aerosol and thermal hydraulics need to be mentioned. One is the change in atmospheric density introduced by high concentrations of aerosols, which may give rise to natural convection currents. The other is associated with the release of decay heat from aerosol particles, either suspended or deposited on walls or in pools. The heat from  $\beta$ - or  $\gamma$ -ray emissions can introduce natural convection currents; it may enhance the superheating of the atmosphere and thus reduce the potential for steam condensation on aerosols; on the other hand, decay heat release may lead to evaporation of water from droplets, water films and pools, thereby increasing the atmospheric saturation and the potential for steam condensation on aerosol particles. Numerical problems are often encountered when modeling the coupled thermal–hydraulic aerosol dynamics, because of some highly transient processes occurring during steam condensation on aerosols. A well balanced method of discretisation in space and time and appropriate iterations for inter-compartment flows, zone-internal processes and heat exchanges with structural walls has to be established to obtain meaningful results.

As discussed previously, many aerosol codes to investigate the aerosol behavior in the containment under severe accident are available (Beonio-Broccheieri et al. 1988). In this study, we have used NAUA Mod 5-M in its present form and have compared the results of the experiments performed for studying metal oxide aerosols interaction with steam.

### **3.1 General**

The NAUA code (Bunz et al. 1983) was developed at KfK around 1983. It is an advanced multi-compartment aerosol behavior analysis code for use in the reactor containments following core-melt accidents. It simulates coagulation, sedimentation, diffusional deposition and steam

condensation on particles. The code uses a numerical representation of the particle size distribution. Thermal hydraulic data must be supplied as input to the code. Simulations are done for a single control volume, where aerosol sources and leakage are taken into account. An extension of the original version is NAUA Mod 5-M (Bunz et al. 1987) for multi-compartment geometries, where the NAUA aerosol simulations are performed for several control volumes. In addition, advective flows between different control volumes are taken into account. Thermal hydraulic conditions and inter-compartment flow rates have to be specified as input data. Thus, NAUA requires the operation of an extra code for containment thermal hydraulics, and does not take into account possible feedback effects which aerosols may cause in the thermal hydraulic conditions. It assumes a well-mixed air-steam atmosphere in the containment.

The NAUA Mod 5M version, used for this study, incorporates the removal of aerosols by diffusiophoresis (essentially Stefan Flow), in addition to the various aerosol processes modeled in NAUA Mod 4 (Bunz et al. 1983). Other versions of NAUA incorporating containment engineered safety features (Gieseke et al. 1986), iodine chemistry (Hosemann 1983), inertial deposition (Sapra et al. 2008) and the behavior of hygroscopic particles (Jokiniemi and Sher, 1987) have reportedly been developed.

### **3.2 Main assumptions of the code**

The following simplifying assumptions are made in the code NAUA;

- (i) Particles are homogeneously distributed in a control volume except for the boundary layer at the walls;
- (ii) Within one particle size class, no difference in particle composition is allowed;
- (iii) Particle properties are functions of only the particle size and of the particle density. These may change due to varying moisture content of the particle;
- (iv) Shape factor and boundary layer thickness are assumed to be independent of particle size.

Internal mixing of species within a size class is assumed to be quickly achieved by coagulation. The spatial homogeneity in the control volume is generally considered to be accomplished by natural convection within the control volume.



### **3.3 Code features**

The removal mechanisms in the code include gravitational deposition, diffusional plate-out, and diffusiophoresis and interaction mechanisms include Brownian coagulation, gravitational agglomeration and aerosol growth by steam condensation. However, the removal of aerosols by inertial, electrical and thermophoretic processes is not included in the code. The code uses a constant diffusional boundary layer thickness of 0.01 cm. The condensation of steam on particles is modeled using the Mason equation (Mason, 1971).

NAUA considers homogeneous co-agglomeration of insoluble solid constituents. Hence, apart from considering water separately, it is a single component code. The particle size used in the code is the volume equivalent radius. Although the code has provision for shape factors, the shape factor for condensation, mobility and agglomeration are normally set to unity. The main strength of NAUA code is that it can follow the build-up of 50 nuclides on size independent basis and can handle size classes ranging from 0.01  $\mu\text{m}$  to 100  $\mu\text{m}$  in 101 size classes. Particle concentrations up to  $10^{-14} \text{ cm}^{-3}$  can be considered. It is a discrete code requiring number-size distribution as input, specified either in the tabular form or as log normal distribution up to two modes. The particles are subsequently tracked using only the total number of size classes and upper and lower limit values. This is unlike the lognormal codes where it is assumed that the size distribution at the end of a time step remains log normal. Other inputs are: aerosol and steam injection rates, containment dimensions, containment thermodynamics and the leak rates. The code output includes time dependent air borne mass concentration, cumulative amount removed by diffusion, sedimentation, diffusiophoresis, leakage and the information on particle size distribution. The porosity of the water-logged spherical agglomerates is accounted for by using an effective density equal to 50% of the actual value. As the code is not integrated with the containment thermal hydraulics, the condensation rates for condensation on particles and the internal wall surfaces are required to be specified as input quantities.

### **3.4 Code validation**

NAUA is a well validated code, both at the level of separate effect experiments in the small NAUA vessel at KfK and also in the integral tests in the Battelle-Frankfurt's DEMONA (Demonstration of Behaviour of Nuclear Aerosols) facility. NAUA is regarded as one of the

most tested and used mechanistic containment codes for aerosol behavior analysis (Kress, 1985; Schoeck and Schikarski, 1985).

### 3.5 Mathematical framework of code

If all the mathematical expressions for the different physical processes are combined, the complete model equation can be obtained as an integro-differential equation, which can be solved only numerically (Bunz et al. 1983, 1987). To facilitate this solution, the particle size distribution expressed by  $n(r)$  is approximated by a number of mono disperse fractions. By this manipulation, the integro-differential equation can be transformed into a system of coupled first order differential equations (Bunz et al. 1983). The form of the equations is as follows:

$$\begin{aligned} \frac{\partial n(r_k, t)}{\partial t} = & S(r_k, t) - [\alpha_d(r_k) + \alpha_s(r_k) + \alpha_l(r_k) + \alpha_f(r_k)]n(r_k, t) \\ & - \sum_{i=1}^N \left(1 - \frac{1}{2} \delta_{ik}\right) K(r_i, r_k) n(r_i, t)n(r_k, t) \\ & + 0.5 \sum_{i=1}^N \sum_{j=1}^N K(r_i, r_k) \beta_{ij}^k n(r_i, t)n(r_k, t) + (1 - \delta_{1k}) \frac{\dot{v}_{k-1}(t)}{V(k) - V(k-1)} \\ & + n(r_{k-1}, t) - \frac{\dot{v}(t)}{V(k+1) - V(k)} \times n(r_k, t) \text{ for } k = 1, \dots, \dots, N, \end{aligned}$$

where  $n(r_k, t)$  is the number concentration of particles of class  $k$  at time  $t$ ,  $S(r_k, t)$  the source of particles of class  $k$  at time  $t$ ,  $\alpha_d$ ,  $\alpha_s$ ,  $\alpha_l$ ,  $\alpha_f$  are the separation coefficients of particles of class  $k$  for diffusional deposition, settling, leakage and diffusiophoresis, respectively,  $K(r_i, r_k)$  is the coagulation probability between particles of sizes  $r_i$  and  $r_k$ ,  $\delta_{ik}$  is Kroenecker's delta ( $=0$  for  $i=k$ ;  $=1$  for  $i \neq k$ ) and  $\beta$  is interpolation coefficient taken as below

$$\begin{aligned} \beta_{ij}^k = & \frac{V_{k\pm 1} - (V_i + V_j)}{V_{k\pm 1} - V_k} && + \text{for } (V_i + V_j) \in (V_k, V_{k+1}) \\ & && - \text{for } (V_i + V_j) \in (V_{k-1}, V_k) \\ & && \text{and } = 0 \text{ otherwise} \end{aligned}$$

$\dot{v}$  is the volume growth rate of particles due to steam condensation and  $V(k)$  the volume of particles of class  $k$ . The equation above is solved by the Euler-Cauchy numerical technique. The time step is calculated internally within the code, using the ratio of the first to the zeroth derivative. This can be shown to be of the same order as the ratio of the second to the first derivative. The above method is applied to the main part of the equation (controlling the coagulation/depletion processes). The time step for the extremely rapid condensation process is calculated by the difference between the result using the full time step and two half steps. If the stability criterion is violated, a smaller time step is assumed and the calculations are repeated.

**Steam condensation in code:** The unique feature of the code is the treatment of steam condensation on the particles which is based on the Mason's equation. This describes the time rate of change in the particle radius due to condensation or evaporation as

$$r \frac{dr}{dt} = \frac{S_{rat} - \exp\left[\frac{2\sigma M}{\rho_w R T_r r}\right]}{\frac{L\rho_w LM}{KT RT} - 1 + \frac{\rho_w R T_\infty}{MDP}}$$

With  $S_{rat}$  = Steam Saturation ratio

$\sigma$  = surface tension of water

$M$  = Molecular weight of water

$\rho_w$  = Specific density of water

$R$  = Universal gas constant

$T_r$  = Temperature of the droplet

$T_\infty$  = Temperature of the gas phase

$L$  = Latent heat of the water

$K$  = Thermal conductivity of the steam

$P_s$  = Steam saturation pressure

$D$  = Coefficient of diffusion of water vapor in air

It is assumed that the ideal gas law holds and that  $T_r$ ,  $T_\infty$ ,  $\sigma$ ,  $\rho_w$ ,  $L$  and  $P_s$  are functions of temperature  $T_\infty$ .

## Chapter 4: Experiments on Harmonization of Particle Measurements

In order to achieve the objectives of the project, experiments have been carried out in three stages. Harmonization of measurements by aerosol instruments of BARC and IITK laboratory has been attempted in the first part. The co-relation factor obtained from this inter-comparison exercise has been applied to estimate the hygroscopic growth of atmospheric aerosols which consequently led to black carbon measurement and modeling. This inter comparison exercise is also important to translate the results of measurements made in one lab to those made in any other laboratory using instruments which work on the same principle. The second part concerns the set of experiments carried out at NATF test vessel at BARC. In these experiments, steam interaction with metallic aerosols has been studied and the results have been compared with NAUA Mod-5 code predictions. The third and final part of the project focused on activation behavior of CsI aerosols in controlled humidity conditions.

This chapter describes the experimental studies and the results obtained for the intercomparison of the measurement systems under varying environmental conditions.

### **4.1 Intercomparison of Scanning Mobility Particle Sizers (SMPS)**

There are several methods available to measure particle concentrations and size distributions of aerosols (e.g. condensation particle counter, electrical low pressure impactor, scanning mobility particle sizer, fast mobility particle sizer etc.). Of these, Condensation Particle Counter (CPC) for number concentration and Scanning Mobility Particle Sizer (SMPS) for size distribution are widely used for environmental and workplace measurements. The counting efficiency and the effective flow rate are required to be known precisely for correct measurements. Also, the uncertainties in these parameters; and knowledge of coincidence error and shifting of counting logic from single particle mode to photometric mode (at high concentrations) should be known, while employing a CPC. The SMPS utilizes a continuous scanning voltage to impart varying mobility to particles and a complex inversion algorithm to deduce the particle sizes from the mobility spectrum. The accuracy of SMPS measured size distribution is governed by several parameters such as the DMA construction, sampling and sheath air flow rates, voltage accuracy,

particle charge distribution, CPC counting efficiency, particle transport time and particle transmission efficiency (Watson et al. 2011). The SMPS is generally calibrated using spherical particles (Mulholland et al. 2006). In most cases, calibration is only with respect to size and not particle concentrations due to the absence of reference particle number concentrations; although a few attempts have been made for the latter (Koch et al. 2008). There are several versions of CPCs and SMPSs available, primarily developed by TSI (Shoreview, MN, USA) and GRIMM (Grimm Aerosol Technik GmbH & Co. KG, Ainring, Germany). The inter-comparability of these commercially available systems has been an important issue of investigation. This is specially so in the context of the data reported in the literature using different versions. Meaningful inferences from these data are only possible if the systems used to measure them are well-evaluated vis-à-vis each other. Some inter-comparison studies have been carried out on size-classifying particle concentration measurement systems (Ankilov et al. 2002, Asbach et al. 2009, Helpser et al. 2008, Watson et al. 2011) but the sampling conditions and the results are not consistent so as to be directly used for the measurements made during the course of the studies carried out under this project.

#### ***4.1.1 Experimental details***

A detailed inter-comparison study of GRIMM-SMPS (model no 5.403) available at Bhabha Atomic Research Center (BARC) and the TSI-SMPS (classifier 3080 with CPC 3775) available at the Indian Institute of Technology, Kanpur (IITK) was performed. This was necessary so as to strengthen the confidence on the aerosol measurements to be carried out as part of this project. Experiments have been carried out under both controlled and ambient conditions. The instruments have been challenged to laboratory test particles (generated by atomization of sodium chloride and ammonium sulphate solutions using TSI 3079 atomizer) and ambient particles, respectively. A more intuitive and appropriate approach for a systematic evaluation of the performances would be to compare the responses of the accompanying CPCs before comparing the SMPSs. This will help in identifying the sub-system which is a likely source of the underlying variations, if any, observed in the SMPS measurements. Hence, as a first level of comparison, only the CPCs of both the SMPSs were compared to a stand-alone TSI-CPC (available with IITK, model no CPC 3776) which was taken as a reference. Subsequently, the second level of comparison was between the two SMPSs. The main aim of this part of the project

was to harmonize the differences observed for SMPS measurements by linking it with CPC differences and other factors such as the role of neutralization efficiencies, inversion schemes etc.

Experiments were performed at Indian Institute of Technology (IIT) campus in Kanpur, India (26.5° N, 80.3° E, 142 m above mean sea level). For comparison with laboratory generated aerosols, a small cuboidal chamber of volume 40 liters with an in-built fan to homogenize the aerosols was used. Sodium chloride (NaCl) and ammonium sulphate ((NH<sub>4</sub>)<sub>2</sub>SO<sub>4</sub>) solutions were used as test aerosols. The chamber had four sampling ports which were judiciously used depending on the context and objective of the experiments performed. The experimental set-up and the SMPS versions are shown in Figure 4.1 (a) and (b) respectively. The lower port of the chamber was connected to an atomizer which was operated at the same air flow rate for all chamber experiments. The atomized aerosols were conditioned using silica bead diffusion dryer before entering into the chamber. One of the upper ports was used with a flow divider to which GRIMM-SMPS, TSI-SMPS (hereafter, referred to as G-SMPS and T-SMPS, respectively) and a TSI-CPC (referred to as T-CPC) were connected. One of the ports was connected to other devices used for other measurements (not part of this study).

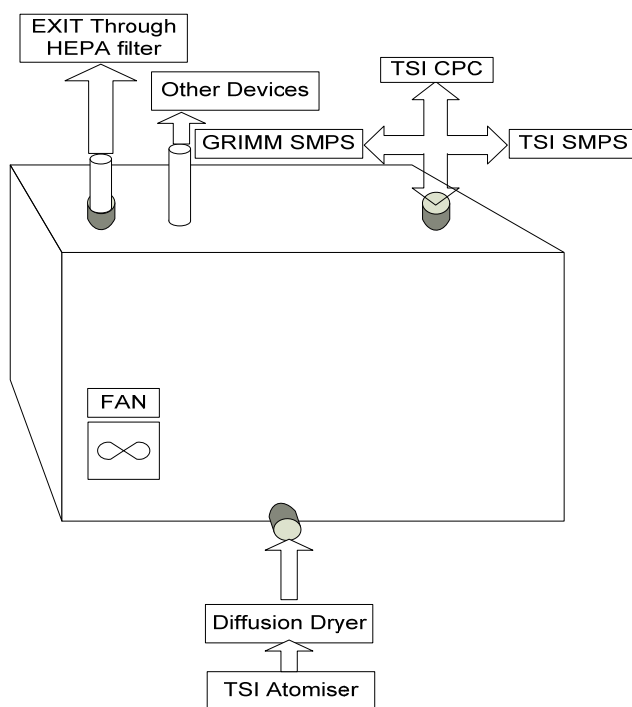


**Figure 4.1 (a):** Experimental set-up used at IITK for intercomparison of aerosol measurements.



**Figure 4.1 (b):** Photographs of Scanning Mobility Particle Sizers used for intercomparisons

The features of the three CPCs and two SMPSs used for experiments are listed in Table 4.1.

**Table 4.1:** Parameters of the SMPSs used in the study

Parameter	G-SMPS	T-SMPS	Stand-alone T-CPC
Model	5.403C	3696	-
DMA	Vienna type	TSI- 3081	-
Aerosol sampling rate ( $\text{lmin}^{-1}$ )	0.3	0.3	-
Sheath air flow rate ( $\text{lmin}^{-1}$ )	3	3	-
Neutralizer	$\text{Am}^{241}$ (alpha emitter)	$\text{Kr}^{85}$ (beta emitter)	-
Diameter range (nm)	11.1 nm – 1083.3 nm	14 - 800 nm	-
Impactor	1185 nm	1282 nm	-
CPC type	Butanol based	3775: Butanol based	3776: Butanol based
CPC maximum concentration	$10^7 \text{ cm}^{-3}$	$10^7 \text{ cm}^{-3}$	$10^6 \text{ cm}^{-3}$
CPC lower limit	4.5 nm	4 nm	2.5 nm
Single particle counting threshold	$1.4 \times 10^4 \text{ cm}^{-3}$	$5 \times 10^4 \text{ cm}^{-3}$	$3 \times 10^5 \text{ cm}^{-3}$

The flow rate at every sampling port was always verified prior to and usually during the experiments. All three instruments were operated at their default flow setting i.e. at aerosol sampling flow rate of 0.3 lpm and sheath air flow rate of 3 lpm. The aerosol exit provided at one port was through a HEPA filter. Electrically non-conducting flexible sampling tubes were used to minimize the losses due to aerosol charges. To avoid ambiguities, similar length (and orientation) of sampling tubes was used for all the instruments being compared, with the tube

length after the flow divider being 0.5 m. Total tube length representing the sampling path was 1 m for each of the instruments. For this length and tube geometry, aerosol losses during tube transit were found to be insignificant. The scan time for distribution measurement was also matched for both the devices. The best available standard protocols (Wiedensohler et al. 2012) were followed for inter-comparison exercises.

For ambient aerosol experiments, sampling was performed on two separate days; February 4-5, 2011 and July 19, 2011. The February sampling was performed overnight while July sampling was during the daytime. For all experiments, TSI data was analyzed using Aerosol Instrument Manager (ver. 7) while GRIMM used SMPS version 1.35 build 1.

The significance of carrying out experiments with both ambient and laboratory generated aerosols was to study the concentration-dependent response of the instruments. For example, Schlatter (2006) showed that the CPC of the SMPS itself accounts for the sizeable differences in the aerosol concentrations reported for values more than  $5000 \text{ cm}^{-3}$ . Below a threshold (see Table 4.1), single count mode with coincidence correction is applied in CPCs while above this concentration; photometric mode is used where calibration is performed with respect to total scattered light intensity. With increase in concentration, shifting of the counting logic to photometric mode can contribute to the differences between CPCs. However, prior to commenting on the concentration related performance, calibration of the systems used in the study using standard particles was undertaken. The results of the experiments performed are discussed here.

#### ***4.1.2 Calibration of SMPSs using standard test particles***

In order to check the sizing accuracy of G-SMPS and T-SMPS, calibration tests were performed in the test chamber. Certified (Duke Standard) Polystyrene Latex (PSL) particles of two different sizes (299 nm and 499 nm) were used in these tests. Atomized PSL particles were injected into the test chamber after passage through the diffusion dryer. After establishing steady state concentration, average size distribution recorded by G-SMPS and T-SMPS was compared. Figure 4.2 presents the SMPS distributions for PSL stated sizes of 299 nm and 499 nm.



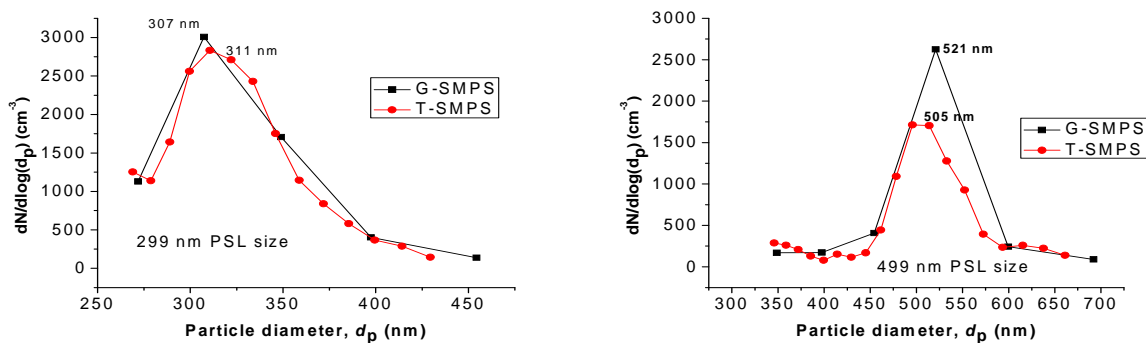


**Figure 4.2:** Calibration of the SMPSs using PSL particles 299nm and 499 nm.

As may be seen, the observed peaks for G-SMPS and T-SMPS were 2.68% and 4.01%, respectively away from the stated PSL size of 299 nm. Similarly, for the 499 nm PSL size, this difference was seen to be 4.41 % and 1.20 %, respectively. Further, we nebulized blank de-ionized water (without adding PSL) and no significant numbers were seen at these stated sizes. Given the uncertainty in the PSL size ( $\pm 2.5$  %) and other possible experimental uncertainties, the results were well within the confidence to proceed further. The calibration of CPC's was not performed for number concentration but their performances for low concentration condition were tested. All CPC's matched well within acceptable limits as will be shown in ambient comparison results.

#### 4.1.3 Intercomparisons using Laboratory generated particles

Prior to comparing the SMPSs, the CPCs of both the SMPSs were compared with the stand-alone T-CPC in the test chamber, using particles generated from atomized sodium chloride solution (0.01 % v/v). Prior to the injection of atomized aerosols, stand-alone T-CPC which recorded  $21172(\pm 1290)$   $\text{cm}^{-3}$  average particle concentration, showed a higher concentration by a factor of  $1.089(\pm 0.096)$  and  $1.049(\pm 0.100)$  compared to CPCs of T-SMPS and G-SMPS. On injection of the test aerosols (concentration measured by stand-alone T-CPC was  $40752(\pm 6452)$   $\text{cm}^{-3}$ ), this factor changed to  $1.177(\pm 0.273)$  and  $1.070 (\pm 0.241)$  for CPCs of T-SMPS and G-SMPS, respectively (Figure 4.3).

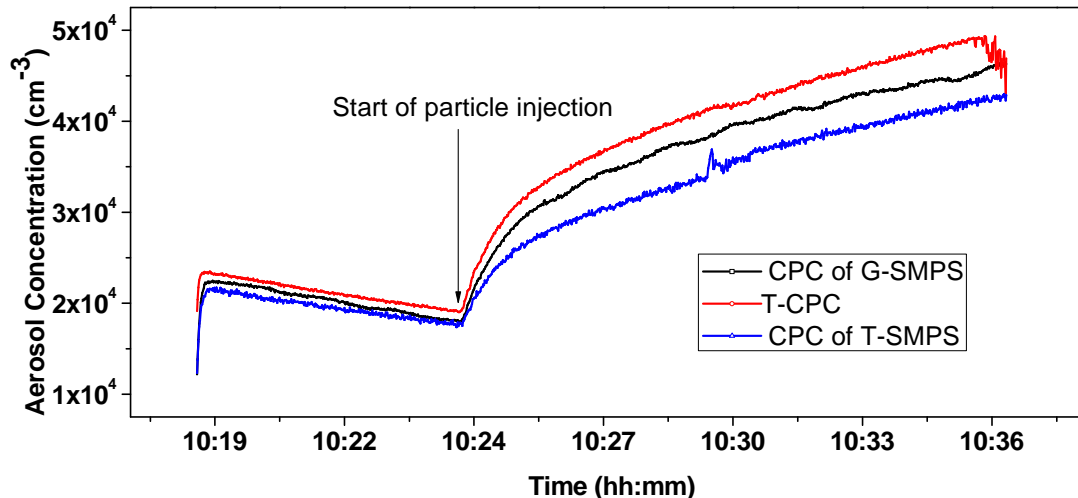


**Figure 4.3:** *CPC comparison for laboratory generated aerosols*

This observation is in agreement with the work of Schlatter (2006) wherein a 5% variation (factor of 1.05) was seen up to 1000 particles  $\text{cm}^{-3}$  which increased to 10% (factor of 1.1) for 10000 particles  $\text{cm}^{-3}$ . A larger variation in the present study is seen owing to higher observed concentrations. The limits of single particle mode counting for these devices are shown in Table 4.1. Considering stand-alone CPC as reference for this case (since it uses single particle counting mode for both concentrations), the factor of difference increased for both CPCs i.e. of G-SMPS & T-SMPS when concentration was increased in the chamber. Since CPC of G-SMPS was measuring concentrations in the photometric mode for both cases (chamber ambient and particle injection), the factor increased slightly from 1.049 to 1.07. Relatively, this factor was higher in case of CPC of T-SMPS since it measured concentrations in single particle mode and transition mode for background and after injection, respectively. The concentration difference factor of the two CPCs (ratio of concentration measured by CPC of G-SMPS and of T-SMPS) increased from 1.038 to 1.095 for the above case. The transition to photometric mode at differing thresholds and the inherent calibration, instrumental and sampling variations contributed to these observed differences. It should also be noted that, both CPCs of TSI had a difference of 8.9% even at lower chamber ambient case which still can be taken as acceptable. It has been shown in previous studies that small changes in instrument settings or flows inside the instruments can contribute to the measurement differences between different systems. For example, even a small change in thermistor settings can cause a difference of concentrations between CPCs (Liu and

Deshler, 2003). So, it is reasonable to accept the variations of different models (of different age) even if they are factory calibrated.

The second step was the comparison of G-SMPS and T-SMPS in controlled chamber conditions using two different types of test particles generated from sodium chloride (0.01 % v/v) and ammonium sulphate (0.03 % v/v) solutions. After conditioning through the diffusion dryer, these were passed into the chamber. The steady state average size distribution for NaCl and  $(\text{NH}_4)_2\text{SO}_4$  aerosols measured by the G-SMPS and T-SMPS are as depicted in Figure 4.4 (a & b).

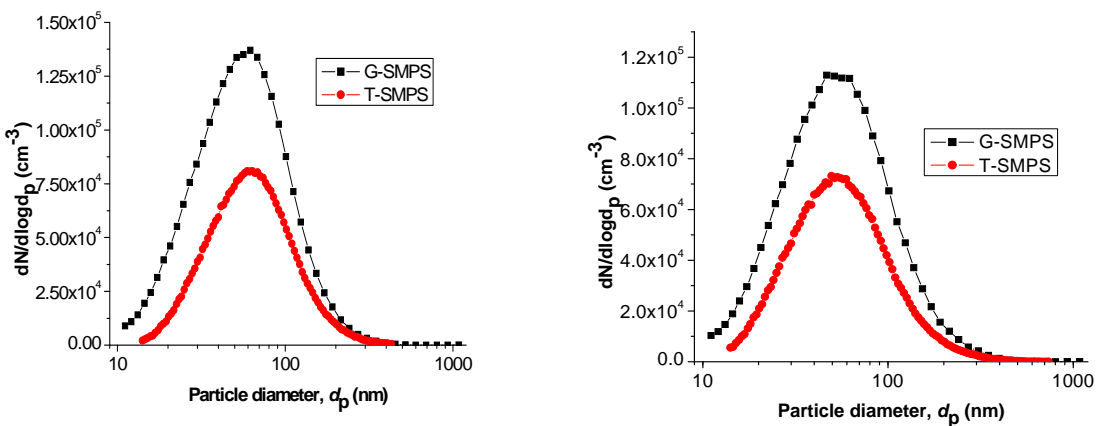


**Figure 4.4 (a, b): SMPS comparison for laboratory generated test aerosols**

For NaCl particles, the geometric means recorded by the T-SMPS and the G-SMPS were 64 nm and 53 nm (G-SMPS 15.6 % lesser than T-SMPS), respectively. The geometric standard deviations obtained from the size distributions were similar at 1.88 and 1.87, respectively. The total number concentrations were compared in the common size ranges of the two SMPSs. It was found that the G-SMPS showed a higher concentration by a factor of about  $1.881(\pm 0.078)$ . For  $(\text{NH}_4)_2\text{SO}_4$  particles, the geometric mean measured by G-SMPS was 10.3 % lesser than the T-SMPS and the total particle concentration was higher by a factor of  $1.725(\pm 0.279)$ . Asbach et al. (2009), in their study on laboratory comparisons with NaCl aerosols, obtained a factor of 1.42-1.7 with GRIMM showing higher number concentrations with almost similar inferences for mean size differences.

An internal analysis of the size-wise variations in the particle concentrations was also carried out and the Relative Concentration Factor (RCF) was estimated as:

$$RCF = \{C_G - C_T\} / C_T$$

Where  $C_G$  and  $C_T$  are the particle concentrations measured by the G-SMPS and T-SMPS, respectively.  $RCF$  is introduced here to compare the results of this study in view of size based differences discussed in the previous studies. As indicated in Table 4.2, larger  $RCFs$  of 4.33 and 1.70 respectively for NaCl and  $(NH_4)_2SO_4$  particles, were observed in the lower size ranges (13-30 nm). These can be compared with the work of Asbach et al. (2009) wherein, factors of up to 2.6 were obtained for lower size ranges. The  $RCFs$  were lower for higher size ranges.

**Table 4.2:** .Size segregated Relative Concentration Factor ( $RCF$ )

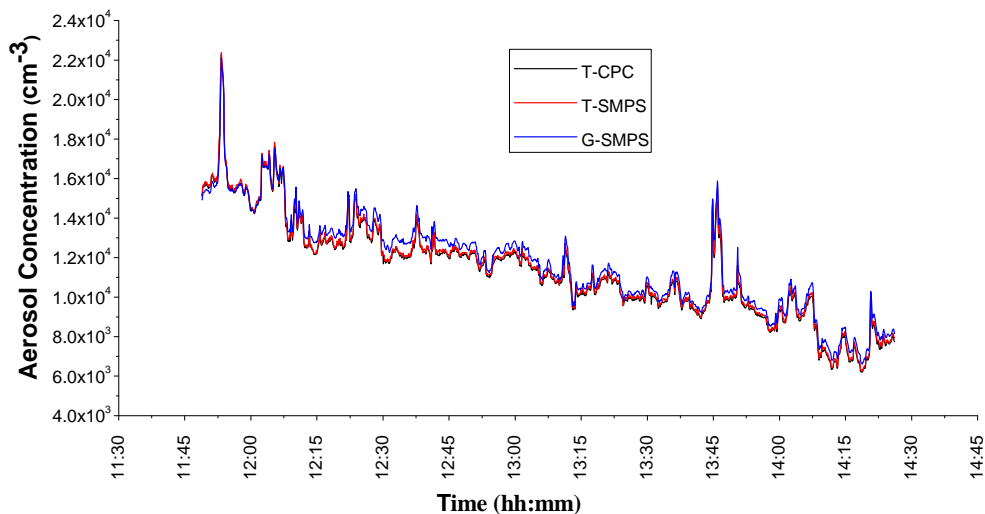
Size Range (nm)	Relative Concentration Factor	
	NaCl	$(NH_4)_2SO_4$
13-20	4.33	1.70
20-30	2.13	1.16
30-50	0.67	0.39
50-70	1.00	0.85
70-100	0.37	0.36
100-150	0.79	0.98
150-200	0.84	1.11
200-300	0.26	0.55
300-400	1.10	1.50

The results for the concentration difference of the SMPSs re-assessed the previous studies carried out for laboratory controlled high concentration conditions. The sources of uncertainty which might be causing these differences have been discussed elsewhere (Wiedensohler et al. 2012, Watson et al. 2012). The most significant might be CPC responses, DMA transfer functions, efficiency corrections, instability of the flows and the differences in neutralized charge distributions. Liu and Deshler (2003) have discussed the effect of aerosol flow changes and insufficient neutralization on the difference between CPC and SMPS. Before examining these aspects, it is worthwhile to also check the differences of CPCs of these units at low ambient concentrations. The next step for our study thus was the comparisons in ambient conditions before attempting the discussion of the above results for the concentration differences.

#### 4.1.4 Comparisons in ambient conditions

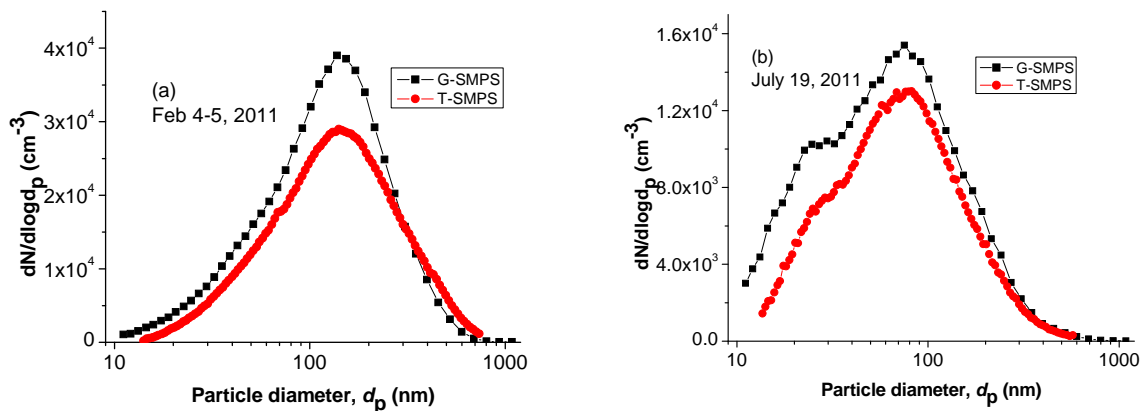
Although in some past studies, efforts were made to check the inter-variations for ambient measurements, we carried out experiments so that the similar systems could be tested for both high and low concentration conditions. This would help us to harmonize the measurements for different concentration conditions. These experiments in ambient environments were conducted during February 4-5, 2011 and July 19, 2011. Firstly, all the three CPCs (T-CPC, CPC of G-SMPS and the CPC of T-SMPS) were compared to check the differences in the total number concentrations recorded by the two instruments.

Figure 4.5 shows the results in the form of time series recorded on February 4, 2011 for a period of about 2.5 h in the ambient environment of IIT Kanpur site. As can be seen, in comparison to higher concentration conditions, as in chamber experiments, CPC variations were low. The CPC of T-SMPS and G-SMPS, respectively showed a factor of  $1.013(\pm 0.014)$  and  $1.047(\pm 0.022)$  times higher concentrations than the stand-alone T-CPC. The average aerosol concentration as measured by T-CPC during this period was  $11,363(\pm 2555) \text{ cm}^{-3}$ . As the concentration was low (below the threshold of single counting mode), close matching of CPCs indicates that coincidence corrected single particle counting for all these CPCs is reasonable.



**Figure 4.5:** CPC comparisons in low concentration ambient conditions

The CPCs were then coupled with their respective DMAs to form the SMPSs. The two SMPS (i.e. G-SMPS and T-SMPS) along with standalone T-CPC were connected to a flow divider and similar protocols as followed during test chamber experiments were followed. However, for ambient comparisons, the tube exit at the other end of flow divider was directly exposed to ambient environment. Figure 4.6 (a) shows a representative size distribution simultaneously recorded by T-SMPS and G-SMPS for February overnight comparison. The geometric mean obtained for the G-SMPS was 122 nm (which was 10.2 % lesser than T-SMPS). However, the GSDs for both the size distributions were similar ( $\approx 2.04$ ). Instead of comparing the total number concentration as provided by the instrument software, we compared the integrated concentrations only for the size range common to both the instruments. With this, results from G-SMPS were found to be a factor of  $1.252(\pm 0.163)$  higher than T-SMPS. Fig. 4.6 (b) depicts the similar result obtained for the comparison on July 19, 2011 performed to check the repeatability of the February results. For this case, the aerosol concentration from G-SMPS was a factor of  $1.161(\pm 0.321)$  higher while the mean was 10.2 % lesser than T-SMPS with almost similar GSD.



**Figure 4.6 (a, b): SMPS comparisons for ambient conditions**

The above results are comparable to those of a recent work by Watson et al. (2011) comparing similar units at Fresno Supersite (ambient) wherein the G-SMPS number concentrations were higher than T-SMPS by a factor of 1.26 (for 10-30 nm) which gradually reduced for the higher sizes finally leading to a trend reversal (T-SMPS > G-SMPS). As observed for low concentration conditions, the G-SMPS number concentration results were approximately 20 % higher than T-

SMPS. A small part of this difference can be linked to the CPC differences ( $\approx 5\%$ ) and the remaining may be attributed to similar factors discussed at higher concentration measurements.

#### 4.2 Harmonization of particle concentration measurements

Based on the results of the measurements as discussed in the previous section (4.1), an attempt to achieve harmonization when measuring particle concentrations using systems from different manufacturers was made. As shown in Figure 4.7 (a), the ratios of the concentrations recorded by CPCs of the two SMPSs to the T-CPC were plotted as a function of the concentration (measured by T-CPC). It was observed that, in concentration range of  $10,000$  to  $40,000\text{ cm}^{-3}$ , concentration ratio for both CPC increased with concentration. However, CPC of G-SMPS (to T-CPC) ratio was seen to be saturating, while that of CPC of T-SMPS was observed to be increasing, in the above stated concentration range. Similarly, Figure 4.7 (b) shows the ratio of the concentrations measured by G-SMPS and T-SMPS as a function of the aerosol concentration (average of G-SMPS and T-SMPS). This ratio increased with increase in aerosol concentration.

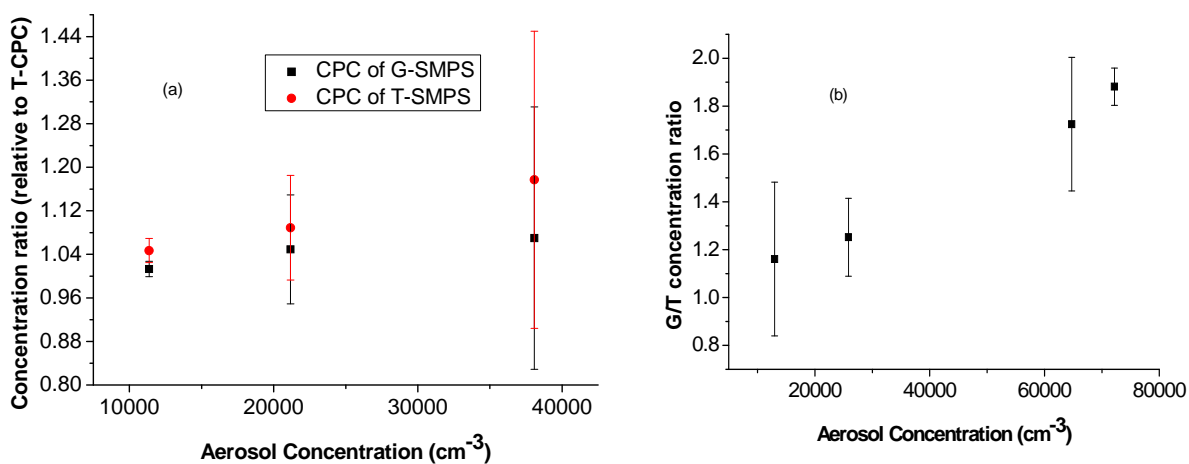


**Figure 4.7 (a, b):** Harmonization of particle concentration measurements

The role of single particle counting mode and the transition effect (to photometric mode) has already been discussed in CPC measurement results. This study also showed that G-SMPS measured higher particle concentrations compared to T-SMPS (consistent with the similar studies performed world-over). For low concentrations, a fraction of this difference may arise due to CPC differences (as observed in our work). While inversion scheme differences were

ruled out as a possible reason, the other possible reasons may be the differences in CPC efficiency curves, diffusion losses and the other sampling variations (Wiedensohler 2012). As the SMPS difference for ambient measurements were not too large for our study, the small differences in device characteristics and measurement uncertainties during measurements can account for the observed response. Considering the above arguments, it seems reasonable to accept the SMPS differences for the ambient measurements.

However, at higher concentrations, the CPC differences became large, but these may not contribute to the large SMPS differences. When the CPC is connected as a part of SMPS, the particles reaching the CPC would be size-segregated and hence at lower concentrations. Hence, the counting mode for this small concentration would be single counting and CPC responses matched fairly well for single counting mode. Then, a possible explanation for the observed SMPS differences is based on the neutralization efficiency of these systems. In comparison to ambient case, the charges produced due to atomization will be large. No additional neutralizer was used in our study except the neutralizers of these devices. An inefficient neutralization would result in higher number concentration as well as lower mean size. Liu and Deshler (2003) demonstrated the effect of such neutralizing inefficiency to explain the larger differences of CPC and SMPS at lower sizes. Since this charging related effect would be prominent for lower sizes, it also explains the larger Relative Concentration Factors (for smaller sizes) observed in our study. The neutralization efficiency can thus be tested for such experiments so as to understand and negate observed effects.

The results of these experiments helped both labs to arrive at a co-relation factor for number concentration and size comparisons. For ambient conditions, these laboratories are using a multiplication factor of 1.2 for converting the total number concentration measured by T-SMPS to mirror it with the G-SMPS. However, in absence of standardized size based interpretations, use of such a relative factor will not be valid for size distributions. Also, at high concentration conditions, more experiments (such as with hydrophilic particles, with lower average charge etc.) are required to discuss and implement such a conversion factor.



### 4.3 Case study: Application to Hygroscopic Growth of Black Carbon Aerosols

Among different types of particulate matter present in the atmosphere, carbonaceous aerosol (black carbon, BC) is the most strongly light-absorbing component of particulate matter (Jacobson 2001), due to its higher imaginary refractive index. These aerosols when emitted have a fractal like chain aggregate structure which makes the calculation of its optical properties quite difficult (Moosmuller, Chakrabarty et al. 2009). A carbonaceous aerosol when coated with other non-absorbing aerosols during ageing shows an increased absorption. This absorption of aged aerosols is 1.5 times greater than fresh aerosols due to chemical processing (Bond, Habib et al. 2006). Enhanced absorption by BC is observed when the atmospheric conditions are favorable for internal mixing (Jacobson 2001). Higher RH with presence of hygroscopic inorganic species makes an ideal situation for the mixing of aerosols creating a core-shell structure having insoluble particles as core and soluble particles as shell. This core-shell structure creates an enhanced absorption in black carbon particles. Absorption enhancement factor of 1.53 in winter for RH between 0% and 99% has been earlier reported (Nessler, Weingartner et al. 2005).

#### 4.3.1 Black Carbon Measurement

Kanpur is situated in the central part of Indo-Gangetic Plain which is classified as one of the most polluted regions in the world. Black carbon measurements are being conducted at Indian Institute of Technology, Kanpur over long time periods. These include BC mass and its absorption coefficient during four winter season starting from 2007. An Aethalometer (AE 42) is used to measure BC mass and Single Wavelength Photo Acoustic Soot Spectrometer (PASS-1) is used to measure BC absorption and scattering coefficients, henceforth referred to as  $\beta_{abs\_exp}$  and  $\beta_{scat\_exp}$  respectively. Figure 4.8 shows the linear regression plot between  $\beta_{abs\_exp}$  and BC mass over four winter seasons. Linear regression coefficients for four consecutive winter seasons (2007-2010) show a very good correlation ( $R^2$ -0.94, 0.85, 0.82 and 0.85, respectively) between  $\beta_{abs\_exp}$  and BC mass. However, the slopes of the regression line show a large inter-annual variation (3.54, 5.77, 14.64 and 17.96 respectively). The higher slope shows an enhanced  $\beta_{abs\_exp}$  measured by PASS-1 for the same BC mass measured by Aethalometer. Since PASS-1 operates on Photoacoustic technique, it does not alter the particle structures and measures the enhanced absorption due to the coating of hygroscopic material over the black carbon. On the

other hand, Aethalometer being a filter-based method measures the absorption due to refractory BC material only upon impacting on the filter and thus underestimates the true absorption.

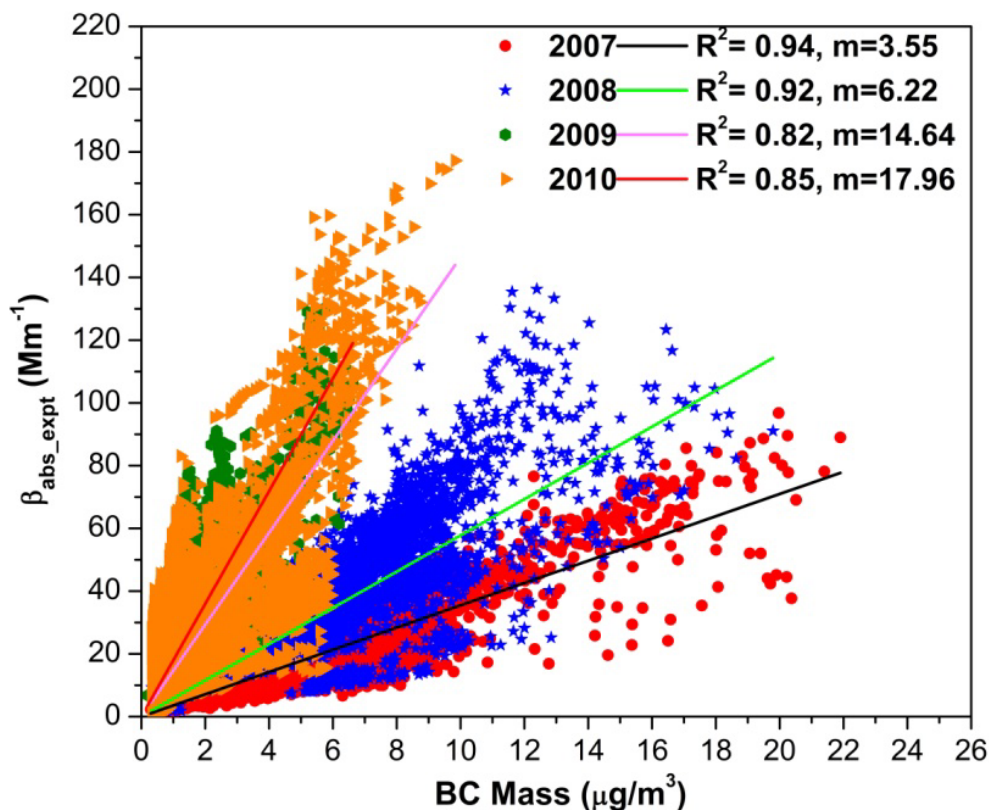


**Figure 4.8:** Linear regression analysis between PASS-1 measured  $\beta_{abs}$  and Aethalometer measured BC mass for four consecutive winter seasons at Kanpur

#### 4.3.2 Experimental Setup

An experiment was conducted from 5 to 10 February 2011 in IIT Kanpur campus to quantify the hygroscopic growth of aerosol particles in the atmosphere and its effects on optical property. The experimental setup consists of two Scanning Mobility Particle Sizer (SMPS), a denuder, PASS-1, Aethalometer and Vaisala Humidcap (HMT 330, Serial No: B4050039) relative humidity (RH) device. Figure 4.9 shows the schematic of instrumental setup used. During the experiment Aethalometer and PASS-1 were operated to measure BC mass and absorption-scattering coefficients (Shamjad, Tripathi et al. 2012). Hygroscopic growth was measured using two SMPS systems in parallel, in which one is connected with a denuder to measure dry particle distribution and the other SMPS is operated in ambient conditions (Aggarwal and Kawamura 2009). The

measured hygroscopic growth factor ( $g_{exp}$ ) is defined as the ratio of the mode mobility diameter of ambient distribution ( $d_{m,wet}$ ) to the mode mobility diameter of the respective dry distribution ( $d_{m,dry}$ ).

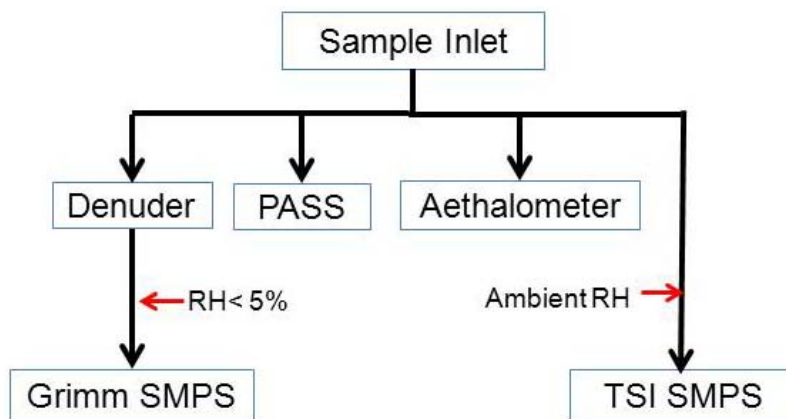


**Figure 4.9:** Schematic of Experimental Setup

### 4.3.3 Calculation of Optical Parameters Using Mie Theory

Scattering and absorbing properties of a particle are also derived theoretically using an analytical approach generally known as Mie theory or Lorenz–Mie theory. Since the analytical calculations are much complex, computer based programs are written to reduce the computational difficulties. The computer program used in this study is known as core-shell code. The core-shell code is developed by Dr. W. Wiscombe, based on the work by Toon and Ackerman (Toon and Ackerman 1981), which is used to compute the scattering and absorption by concentric spheres. Major inputs to the code are the wave number, radii of core and shell, and their refractive indices. The wave number is defined as  $(2\pi/\lambda)$  where  $\lambda$  ( $=0.781 \mu\text{m}$ ) is the wavelength at which the calculations are done. Upon executing the code, it produces absorption ( $Q_{abs}$ ) and scattering efficiencies ( $Q_{scat}$ ) for a single particle. The computed  $Q_{abs}$  and  $Q_{scat}$  for mono-disperse particle needs to be integrated for a whole range of radii to get the net optical properties of poly-disperse aerosol. Aerosol chemical composition is required for accurate modeling of optical properties of aerosol. The method of Kreidenweis et al. (Kreidenweis, Petters et al. 2008) is followed in the present study to estimate aerosol chemical compositions.

#### 4.3.4 Quantification of Hygroscopic Growth

To check the consistency of both SMPS's distribution, they were operated under similar conditions. Figure 4.10 (a-e) shows the resulting distribution. They show very similar mode diameter (within 2%) and geometric standard deviation (within 1%) (Joshi, Sapra et al. 2012). Hygroscopic growth factors for ambient aerosols were calculated from hourly averaged SMPS data. A total of 33 hourly samples were used in this study. The measured hygroscopic growth has values ranging from 1.01 to 1.25. Dry and ambient size distributions for the high RH (Figure 4.10 (b, c)) and low RH (Figure 4.10 (c,d)) are shown below. It is found that not only RH but the presence of hygroscopic species is also responsible for higher or lower hygroscopic growth. Hygroscopic species like  $(\text{NH}_4)_2\text{SO}_4$  and  $\text{NH}_4\text{NO}_3$  are prone to enhance the hygroscopic growth.

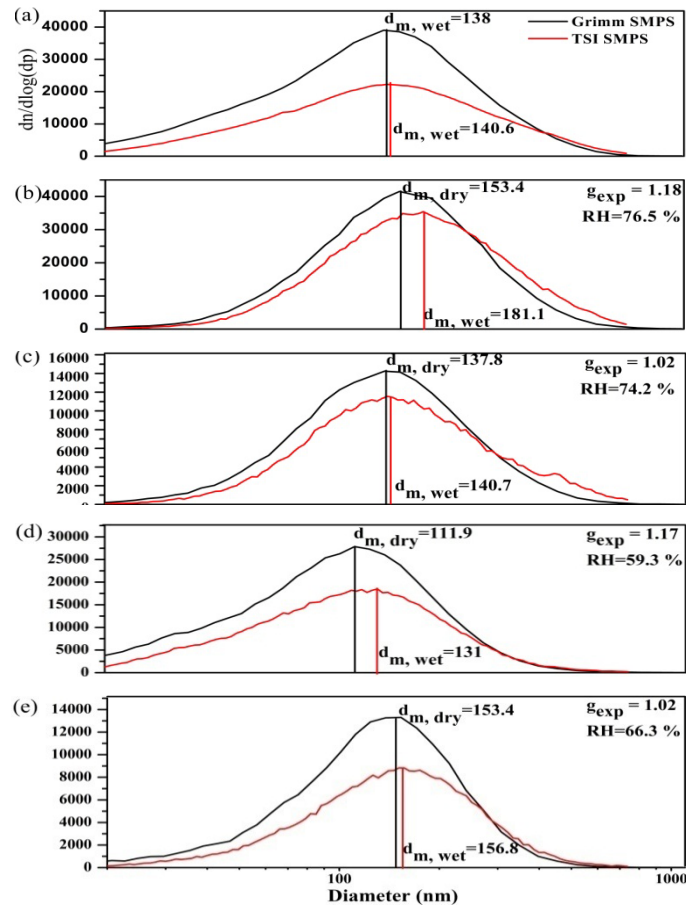


**Figure 4.10:** Aerosol size distribution measured by Grimm SMPS and TSI SMPS for (a) in similar ambient condition, (b) when GRIMM was connected with a dryer and RH = 76.5 %, (c) same as (b) but for RH = 74.2%, (d) same as (b) but for RH = 59.3%, and (e) same as (b) but for

$RH = 66.3$ .  $d_{m,dry}$  and  $d_{m,wet}$  are dry and wet mode diameters, respectively and  $g_{exp}$  is the growth factor (Shamjad, Tripathi et al. 2012)

#### 4.3.5 Analysis of Optical Properties

Optical properties measured during the experiment were compared with that of core-shell code. Figures 4.11 and 4.12 show the comparison between modeled and experimental optical parameters. Figure 4.11 compares  $\beta_{abs\_model}$  and  $\beta_{abs\_exp}$ . The difference between the two is always less than 5%. Figure 4.12 shows the comparison between  $\beta_{scat\_model}$  and  $\beta_{scat\_exp}$ . The difference between modeled and measured scattering coefficient (less than 30%) is higher than that in absorption coefficient.

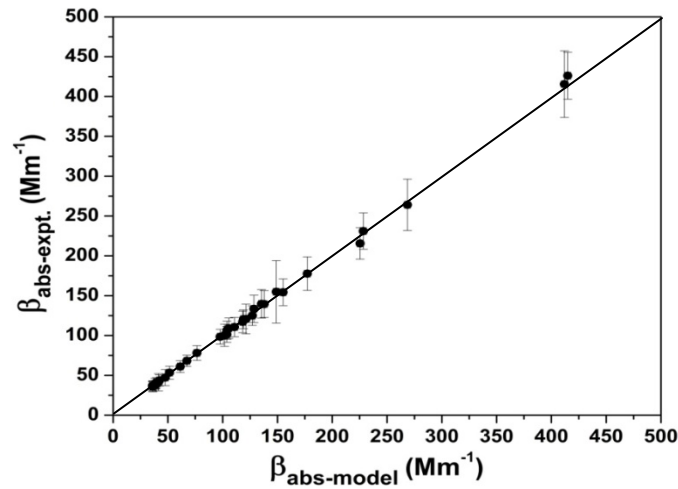


**Figure 4.11:** Comparison of  $\beta_{abs}$  obtained from experiment and Mie Calculations

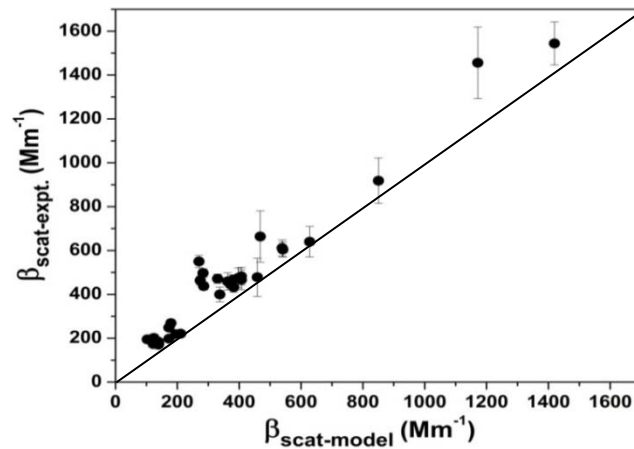


**Figure 4.12:** Comparison of  $\beta_{scat}$  obtained from experiment and Mie Calculations

### 4.3.6 Absorption Amplification

Absorption amplification ( $\gamma$ ) is defined as the ratio of  $\beta_{abs}$  of core and shell to  $\beta_{abs}$  of core alone. Earlier studies have found  $\gamma$  varying from 1.5 to 20 for different monodisperse core and shell configurations (Bond, Habib et al. 2006). But in this study, for a poly-dispersed aerosol system this enhancement gets reduced due to the damping of cross-section oscillations (Nessler, Weingartner et al. 2005). Another reason for the high  $\gamma$  values in Bond et al. (Bond, Habib et al. 2006) is due to the very high values of shell thickness used in their calculations compared to those observed in the present study. It is observed from the current experiment that the shell thickness due to hygroscopic growth is much lesser. In the present study the measured shell thickness vary from 1 to 18 nm. Figure 4.13 shows the variation in  $\gamma$  as function of BC mass fraction and shell thickness. Where BC mass is taken from Aethalometer and PM1 (particulate matter less than 1 microm) mass is taken from corresponding SMPS distributions. This figure shows a clear trend of increase in absorption enhancement as the BC mass and shell thickness increases. A maximum  $\gamma$  value of 2.3 is observed for the shell thickness of 18 nm. The lowest  $\gamma$  value of 1.035 corresponds to very thin coating. It is found from the plot that even for very high BC mass fraction the enhancement in absorption will be predominant only when there is sufficient soluble material available for coating. In such cases even a much less amount of BC can produce high absorption. Considering the entire hourly data an average absorption enhancement of 1.42 is found (Shamjad, Tripathi et al. 2012).

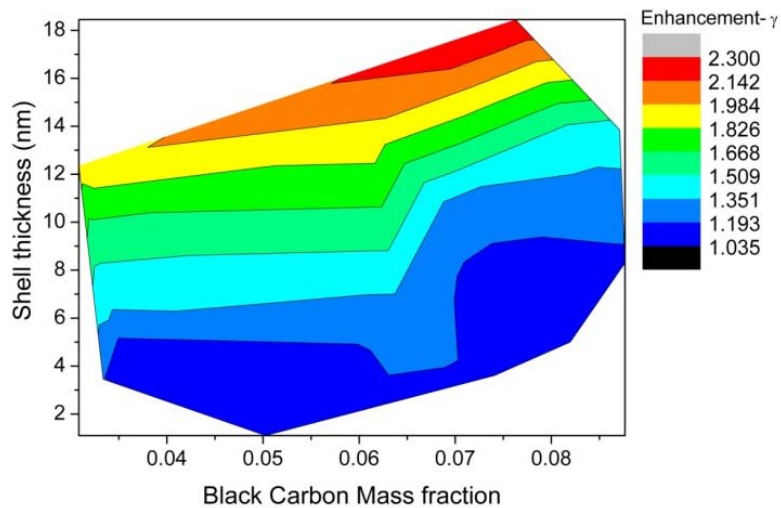


**Figure 4.13:** Absorption enhancements with respect to BC mass and shell thickness

Our analysis based on PASS-1 and Aethalometer data over four consecutive winter seasons shows that  $\beta_{abs}$  of black carbon is highly dependent on RH and other inorganic species. In high RH conditions these inorganic species mix with available water content which forms a coating over the black carbon. This core-shell structure is primarily responsible for the enhanced absorption properties of black carbon. Measurement of hygroscopic growth is found to be very useful in deriving the concentration of different aerosol species present during the time of experiment. Concentration of these species derived from hygroscopic growth is close to the filter based measurements done by Kaul et al, 2011 in the same location (Kaul, Gupta et al. 2011).

## Chapter 5: NATF Experiments- Aerosol Steam Interaction

The aim of these experiments was to study the containment behavior of plasma torch generated metal oxide aerosols in presence of steam. These experiments have been attempted for the first time in the Indian context. The important fact which stands out with regards to these experiments is the deployment of instruments which measure number characteristics of aerosols. The dynamics of containment aerosols in past experimental facilities has mostly been studied with respect to mass measurements. Present set of experiments focused on measuring aerosol characteristics as well as droplet characteristics, simultaneously. These included initial experiments to assess the spatial and temporal thermal conditions in presence of steam. All the experiments discussed in this chapter have been performed in the NATF test vessel ( $\sim 10 \text{ m}^3$  volume) simulating the nuclear reactor containment.

The experimental conditions, results of experiments and comparisons with the NAUA code predictions are presented in this chapter.

### 5.1 Temperature profile in the test vessel in the presence of steam

Using plasma torch aerosol generator, metal oxide aerosols were injected into the containment vessel (volume  $10 \text{ m}^3$ ) and the aerosol number concentration and mass concentration was measured at different locations, temporally. Peak aerosol number concentration of approximately  $3 \times 10^6$  per  $\text{cm}^3$  and peak mass concentration of approximately  $0.2 \text{ g/cm}^3$  was measured. After establishing uniform aerosol conditions in the vessel, steam was injected for about 90 seconds. Four thermocouples were installed at different locations (to check the temperature of the bulk gas and near the wall) and the response was recorded during aerosol generation period (plasma torch on), steam injection period (plasma torch off, steam feeding on) and thereafter (after filling the chamber with steam). The temperature profile in the containment vessel (bulk) is represented in Figure 5.1 below.



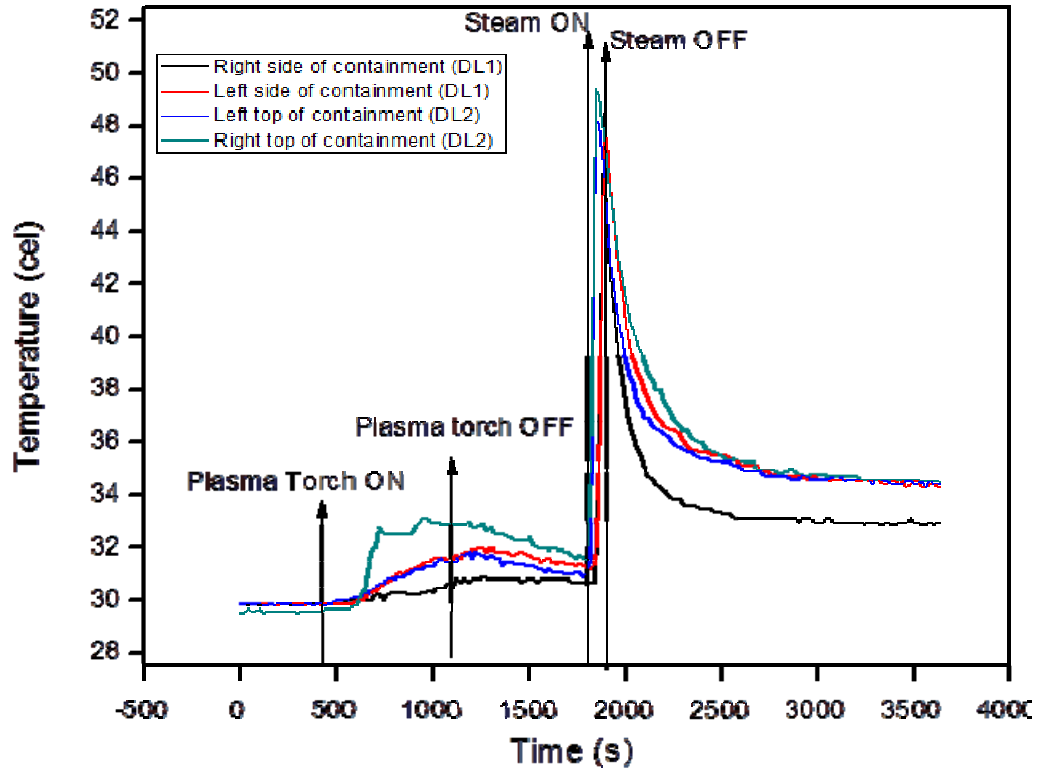


*Figure 5.1: Temperature profile (bulk) in test vessel during aerosol generation and steam feeding*

It is apparent from the above figure that, the maximum bulk temperature reached during the experiment was around 48°C and thermocouple recordings convinced that after saturating vessel with steam and then switching off steam input flow, temperature falls to about 45°C within 600 s and is thereafter stable for a considerable time. This exercise was undertaken to understand the relationship between time and temperature gradient of chamber in presence of steam environment. This information was important for operation of the most vital instrument for the measurement of droplet concentrations, namely, the Cloud Droplet Probe. As per the specifications of this system, the optimal temperature of the sampling stream input to this system should be below 45°C. It may be noted that, the although initial temperature conditions during varying sets of experiments may be slightly different due to change in enthalpic parameters, nevertheless, depending on online temperature recordings, suitable time to start the CDP can be adjusted for every experiment.

## 5.2 Experimental protocol

A few pilot experiments were performed to standardize the NATF parameters and to evolve a common protocol for conducting experiments and measuring required characteristics taking care of constraints of sampling and instrumentation. On the basis of these experiments, the evolved and followed protocol is stated below:

1. Plasma Torch (PT), Powder feeder, aerosol transport tubes and the containment was thoroughly cleaned before and after each experiment.
2. Plasma torch was operated for 15-20 min with sample feed rate of  $\sim 1$  g/min with the following operating parameters.

*Table 5.1: Operating conditions of plasma torch aerosol generator*

Torch Power	10 KW
Current	200 A
Voltage	50 V
Primary Plasma gas	Argon (25 lpm)
Secondary Plasma gas	Nitrogen (2.5 lpm)
Powder feed rate	$1 \text{ g} \cdot \text{min}^{-1}$
Powder carrier gas	Argon (10 lpm)
Diluter /aerosol carrier gas	Compressed air/Argon (100 lpm)

Under these operating conditions, few gross air filter paper sampling measurements were also performed and a peak mass concentration of approximately  $0.1 \text{ g/m}^3$  was obtained. However, while using mass parameters for comparison of experimental observation with code predictions, mass concentration was estimated from the number concentrations which were measured by SMPS and Aerodynamic Particle Sizer (APS) for all experiments. Size distributions for experiments were also measured with SMPS and APS (no impactor used) for number distributions. In one experiment, the operating conditions of the plasma torch were tuned to produce relatively higher number concentration.

3. During the material feed to the Plasma Torch (PT) i.e. during aerosolization, aerosol size distribution was obtained using SMPS and APS (covering 10 nm-20  $\mu\text{m}$ ). CPC was connected in chamber to measure integral number concentration of aerosols ( $> 4.5 \text{ nm}$ ).
4. After about 20 minutes of plasma torch operation, aerosol generation was stopped and steam was injected into the containment for about 1-2 min at 35g/s so as to limit the peak temperature of the vessel up to 65 °C. Total steam content in the containment was decided based upon the fact that the CDP cannot be operated above 40-45 °C and if the temperature of the vessel is increased to a higher value, valuable initial data will be lost. However, the vessel was seen to be saturated due to steam which was also verified from RH measurements (RH close to 100 % in presence of steam). During steam injection, no instrument was operated.
5. When the temperature of the vessel dropped to approximately 45 °C, CDP was operated to obtain the droplet parameters (number, mean size, liquid water content).
6. Once the LWC measured by CDP became sufficiently low, other aerosol instruments were operated again (CPC, SMPS, APS). Sampling from CDP was also discontinued once the LWC became too low.

Total duration for each experiment was 2-3 hours and six experiments were performed under this project. Details of these experiments are presented in Table 5.2.

***Table 5.2: Details of NATF aerosol-steam experiments***

<b>Name of experiment</b>	<b>Date</b>	<b>Aerosol</b>	<b>Steam</b>	<b>Fan status after steam</b>
Experiment 1 ( <b>E1</b> )	14 <sup>th</sup> Aug 2012	Tin oxide	ON	OFF
Experiment 2 ( <b>E2</b> )	10 <sup>th</sup> Aug 2012 (AN)	Zinc oxide	ON	OFF
Experiment 3 ( <b>E3</b> )	10 <sup>th</sup> Aug 2012 (FN)	Zinc oxide	ON	OFF
Experiment 4 ( <b>E4</b> )	9 <sup>th</sup> Aug 2012 (AN)	Zinc oxide	ON	ON
Experiment 5 ( <b>E5</b> )	9 <sup>th</sup> Aug 2012 (FN)	Zinc oxide	OFF	ON
Experiment 6 ( <b>E6</b> )	8 <sup>th</sup> Aug 2012	Ambient	ON	OFF

In all these experiments, fan was kept on in absence of steam (i.e. during operation of plasma torch to homogenize aerosol in the vessel). E1, E2 and E3 have been performed for studying the behavior of metal oxide aerosols in NATF chamber in presence of steam. In E4, fan was kept on so as to understand the fan induced turbulence in presence of steam for almost similar aerosol conditions. An experiment was also performed (E5) without injecting steam while steam interaction with ambient aerosol was studied in E6.

Figure 5.2 shows a time series for a typical experiment E1 showing a sequential progression of experiment and associated measurements. Table 5.3 shows the time profiling for the same experiment.

**Table 5.3: Time profiling for experiment E1**

Time	Event
14:33	Expt. Started- Measurement of chamber background
15:18	Plasma torch on with zinc metal powder-Fan on
15:30	Plasma torch off-Fan off
15:31	Steam on
15:32	Steam off
15:35	CDP on
15:54	CDP off
15:56	APS +SMPS on
17:46	First set experiment completed

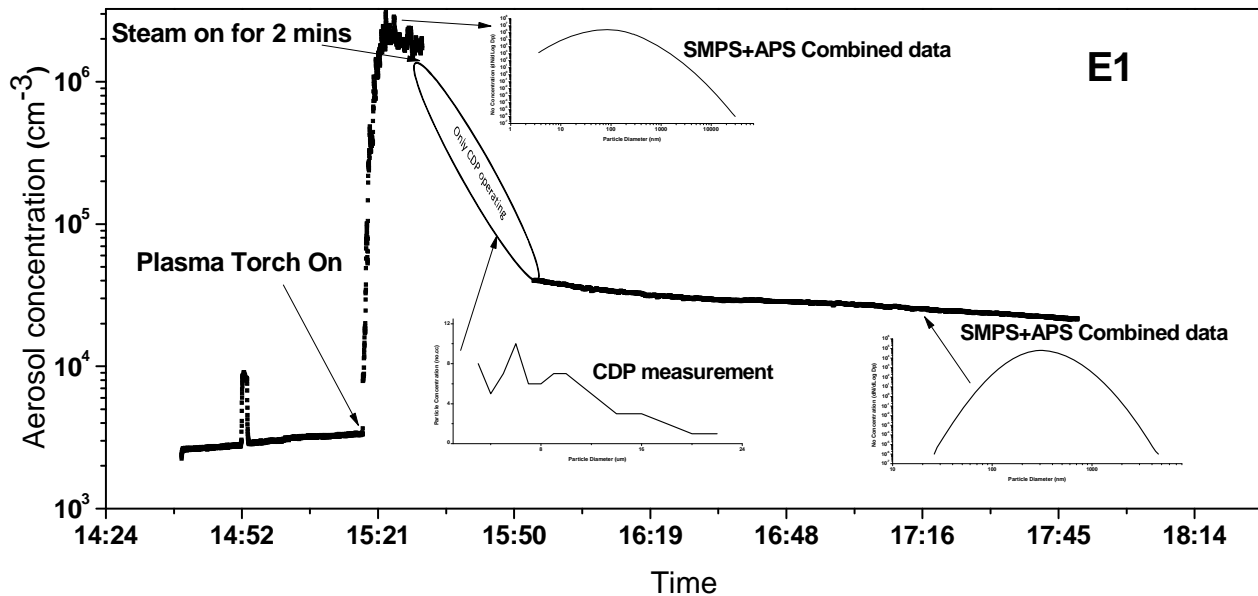


**Figure 5.2: A complete time series for experiment E1 (with Tin oxide)**

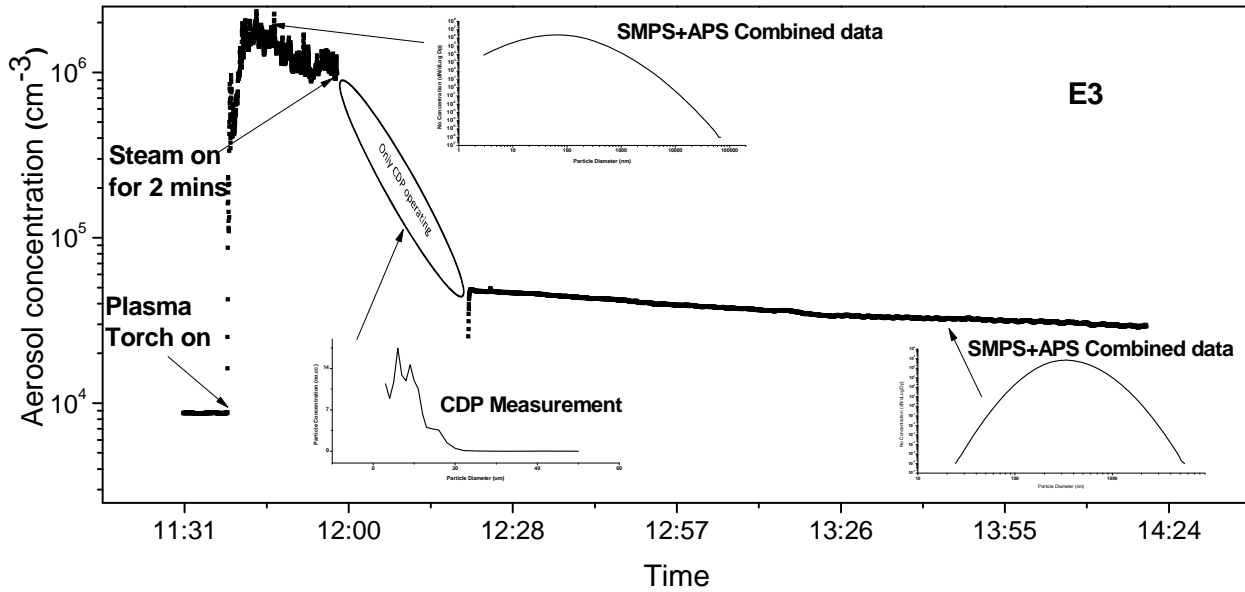


**Figure 5.3:** A complete time series for experiment E3 (with Zinc oxide)

It may be seen from the figure that, before injecting steam, the number concentration generated by the plasma torch was measured by CPC while the merged distribution measured by SMPS and APS was taken as the representative size distribution. Just before PT was switched off (and steam was inserted), steady state (or average) mean size of aerosols was noted (before 12:00 in above figure). After the test vessel became saturated with steam, no instruments were operated for some time due to high temperature and RH conditions. However, as soon as the temperature of the test vessel became less than 45°C, CDP sampling was started. This intermediate period had high water content in the test vessel and the parameters such as droplet distribution, mean volume diameter and liquid water content were measured by the CDP. Once the water content in air became low enough, CPC, SMPS and APS were operated again to provide number concentration and size distribution of the processed aerosols (aerosols remaining after condensation effects). As also seen, slow decrease of number concentration in the above time series means that the processed aerosol conditions are almost uniform afterwards. Figure 5.3 shows a similar time series for E3 (experiment with Zinc oxide aerosols).

## 5.3 Experimental Results

### 5.3.1 Aerosol size distributions

For all experiments, SMPS measured the aerosol mobility size distribution in the size range of 14-800 nm while APS measured aerodynamic diameter from 500 nm-20  $\mu\text{m}$ . For merging these two different distributions in the common range, merging software TSI aerosol manager was used. Figure 5.4 (a, b) shows the change in size distributions for experiments of E1-E3 due to effect of steam.

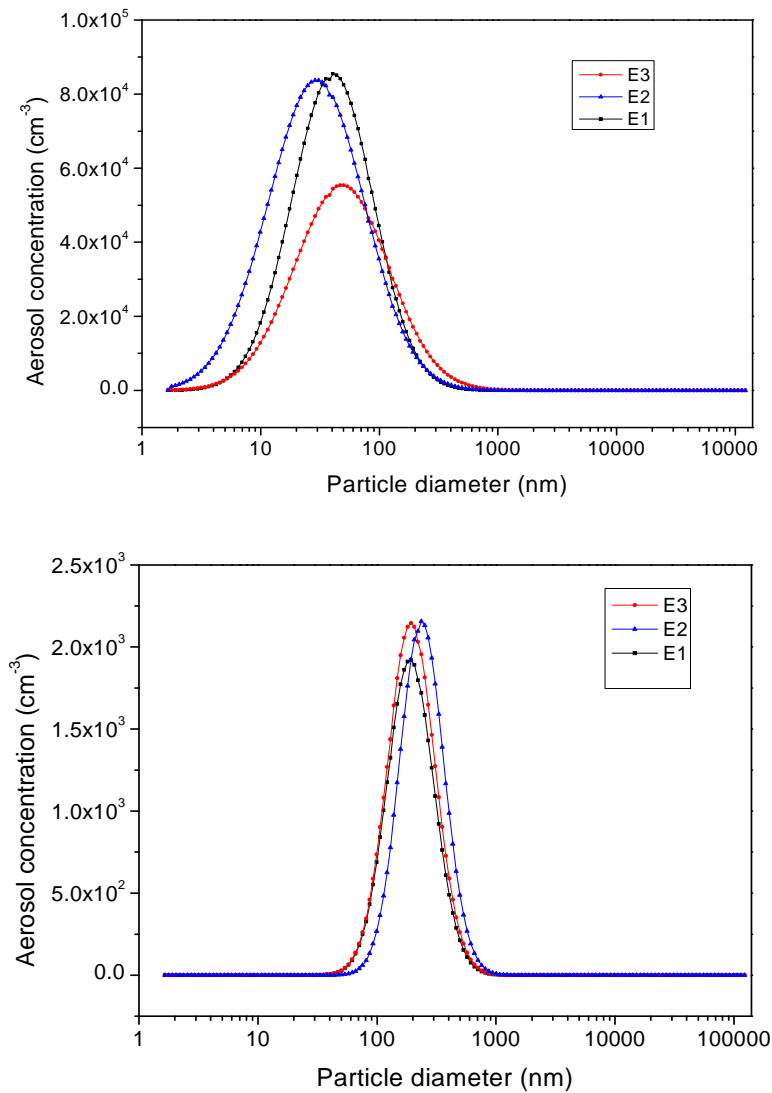


**Figure 5.4:** Steady state aerosol size distribution a) before and b) after steam for experiments E1, E2 and E3

It may be seen from the above figure that the pre-steam average parameters for zinc and tin oxide aerosols were not very different and almost similar aerosol distributions for processed aerosols were obtained for all experiments. The mode diameter for zinc oxide aerosols (E3- 67 nm, E2- 55 nm) changed to approximately 300 nm (for both), respectively. For tin oxide aerosols (E1), mode diameter changed from 86 nm to 300 nm as an effect of steam action. As is seen, although there were minor differences in mode diameters of the pre-steam seed aerosols, the post-steam processed aerosols showed a similar mode size of about 300 nm.

### ***5.3.2 Measurement of Droplet Parameters***

The enhanced feature of these experiments is the measurement of droplet parameters. Figure 5.5 (a, b, c) shows mean volume diameter (MVD), liquid water content (LWC) and droplet number concentration (DNC) for E1-E3. As could be seen from these figures, the condensational behavior of aerosols in presence of steam was significantly different for zinc oxide and tin oxide aerosols. All droplet phase parameters i.e. MVD, LWC and DNC were found to be higher for tin oxide aerosols in comparison to zinc oxide aerosols. The water absorption behavior of aerosols is a strong function of chemical composition as well as physical parameters (size). For a certain RH condition and chemical composition, Kohler theory (Kohler, 1936) predicts a critical diameter above which the drop becomes activated (i.e. continuously grows in size). Since, the physical parametric conditions (mean size before steam conditions) for zinc and tin oxide experiments were maintained same (using similar plasma torch conditions), the differences observed in the droplet phase parameters can be attributed mainly to hygroscopicity.

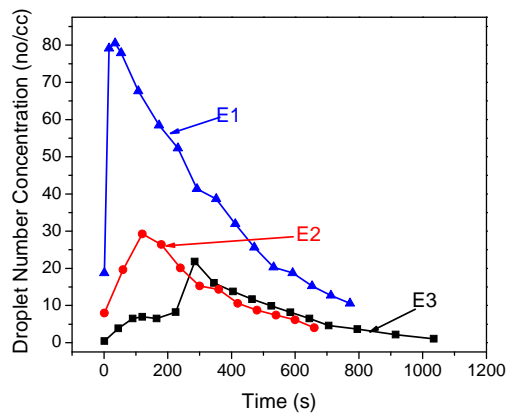
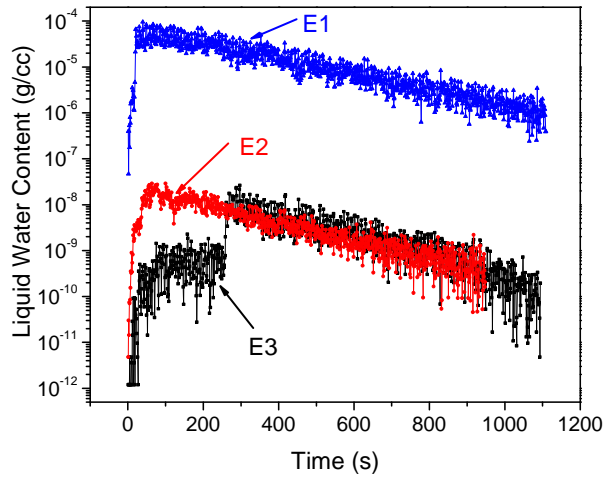
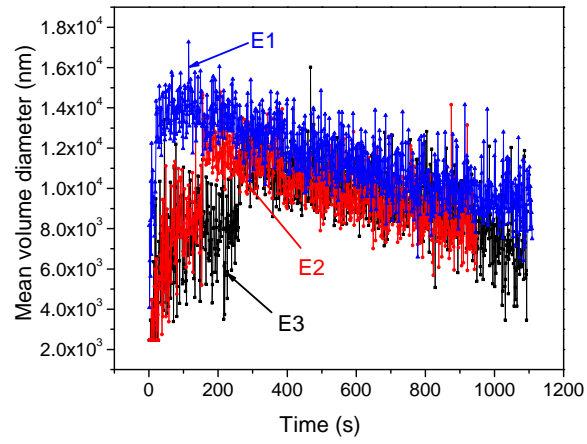


*Figure 5.5 (a, b, c): MVD, LWC, DNC measured by CDP (for experiments E1-E3)*



As observed in terms of CDP measured parameters, the behavior of zinc oxide (E3, E2) was seen to be different from tin oxide (E1). Tin oxide aerosols were observed to have higher MVD, LWC and DNC in comparison to zinc oxide aerosols.

As an interesting insight, temporal reduction in number concentration of zinc oxide aerosols of E3 and E2 can be compared with E5 wherein the plasma torch generated aerosols were allowed to decay in absence of steam (Figure 5.6). However, the initial number concentration and geometric mean diameter for this experiment (E5) was tuned to higher values (number concentration  $\approx 10^7 \text{ cm}^{-3}$ , mode-225 nm). As may be noted for E5, the rate of decrease of number concentration was faster than that for E3 and E2 which is attributable to increased rate of coagulation in case of E5 where the number concentrations were higher. However, as one order increase of number concentration (for ultrafine aerosols) may not affect the mass concentrations, a temporal mass measurement would be expected to provide a different result for such conditions. This points to the fact that mass measurements made with air sampling may have missed this difference. This clearly highlights the need and importance of knowing particle number characteristics for experimental analysis and code simulations.

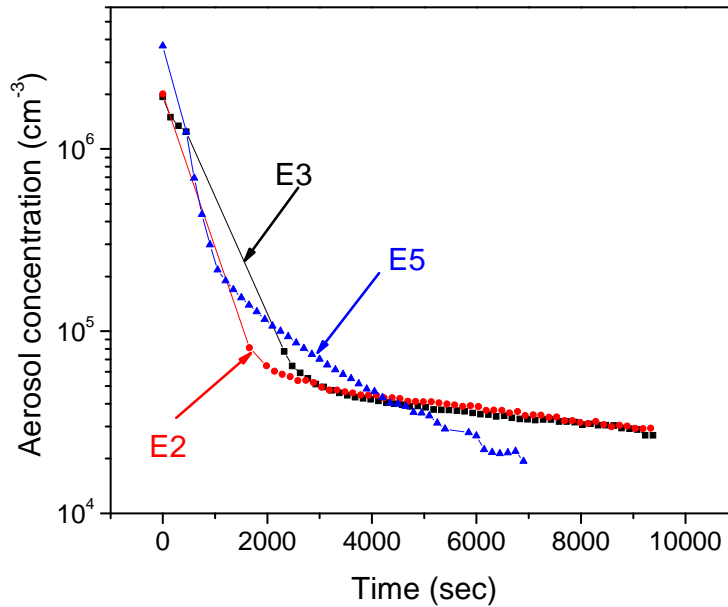


**Figure 5.6:** Comparison of particle depletion rates in E3 & E2 with E5

As the initial mean size of E5 (225 nm) was significantly different compared to other experiments, it would be wrong at this point of time to attribute the change in decay rates to condensation effects. To see the effect of turbulence, in experiment E4, fan was kept on during the steam injection and subsequent times. As may be seen from Figure 5.7, LWC was found to be lower than other steam experiments due to steam depletion because of increased turbulence.

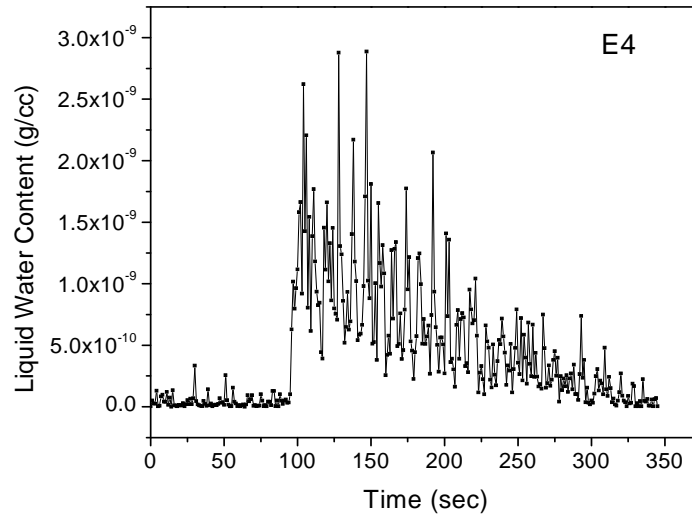


*Figure 5.7: LWC in presence of turbulence measured by CDP for E4*

#### 5.4 Comparisons with NAUA Code

The results of these experiments have also been compared with NAUA MOD 5 predictions. The input conditions and their sources for comparing code with experimental results are stated below:

1) Steam conditions:

Steam flow rate: Calculated from RH-temp conditions, wall condensation rate- 10 %

2) Thermal conditions:

Temperature: Measured with thermocouples

3) Aerosol parameters:

Total aerosolized mass, geometric mean size, geometric standard deviation: Measured with SMPS and APS, density- half oxide density

4) Other parameters:

### Leakage rate, shape factors, vessel parameters- fixed

Steam and thermal conditions were almost similar for all experiments while aerosol parameters were taken as per actual measurements using the merged distributions. Other parameters were kept same during code runs. Figure 5.8 shows the comparison of number concentration of test vessel aerosols (CPC actual and SMPS integrated) in presence of steam for E3.

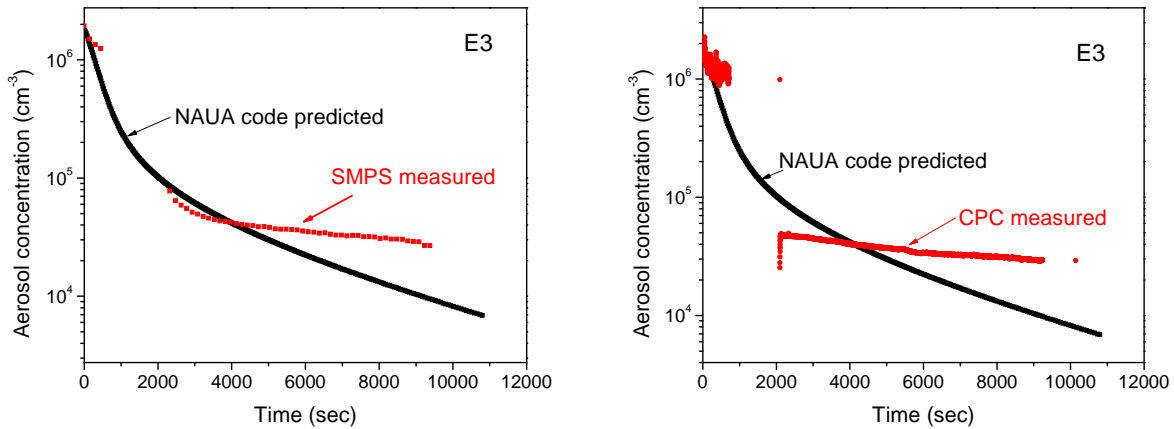


**Figure 5.8:** Experimental and code predicted number concentrations by SMPS and CPC for E3

As may be seen from this figure, code predictions were close to the experimental results. However the uniform concentration seen in experimental results was due to gravitational stratification effects. These measurements were made at 1 meter sampling height where similar kind of uniformity has been seen in earlier studies (Sapra et al. 2008) compared to relatively faster depletion at top end of vessel (See Fig. 9 of Sapra et al. 2008). Considering entire volume of vessel (with height of 3.5 m), the average behavior for number concentration is expected to be much closer to code predictions. Such ambiguities can be largely controlled by using a fan for homogenous mixing but in these experiments, fan could not be used for maintaining steam conditions. A separate model can however be used to incorporate such stratification effects in lines similar to that discussed in Mayya et al. 2005. For experiments E2 and E1, similar kind of inferences can be drawn for experiment-code comparisons (Figures 5.9 and 5.10)

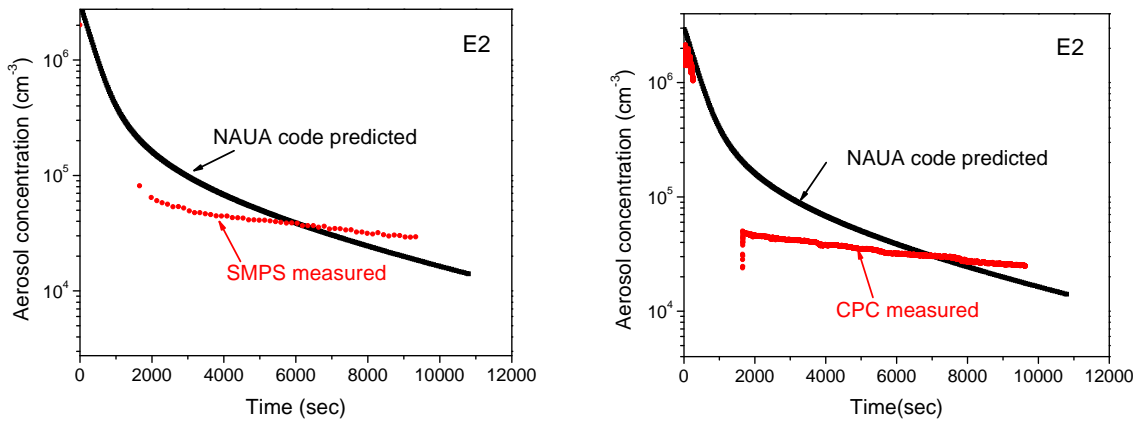


**Figure 5.9:** Experimental and code predicted number concentrations by SMPS and CPC for E2

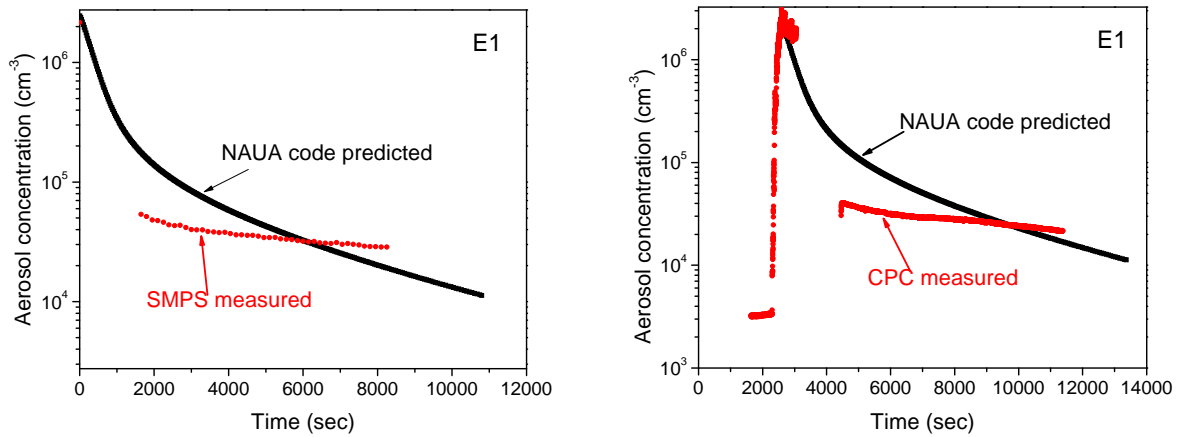


**Figure 5.10:** Experimental and code predicted number concentrations by SMPS and CPC for E1

For experiment E5 where no steam was injected, dry run was made with the code to check the consistency. As evident for no steam conditions and as per measured input aerosol conditions, the code predictions were found to be reasonably closer to be experimental results. Also, presence of fan during the entire experiment negated the gravitational stratification effects thus showing a depleting aerosol concentration (not uniform as for E1-E3).

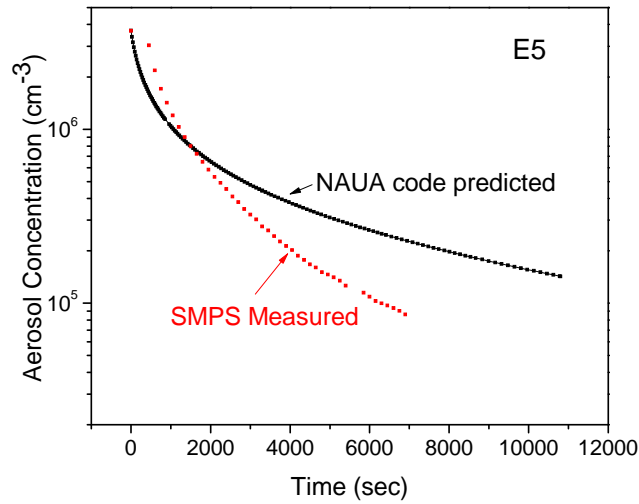


**Figure 5.11:** *Experimental and code predicted number concentrations for E5*

For these experiments, size distribution changes have also been compared with code predictions. However, for the code predictions could only be compared for later times, as size distribution measurements were not possible in the early phase of steam injection. Hence Fig 4.25 and 4.26 shows the size distribution comparison for E1 and E3, respectively. Results for E2 were almost similar to E1 and hence have been left out for the present comparison.

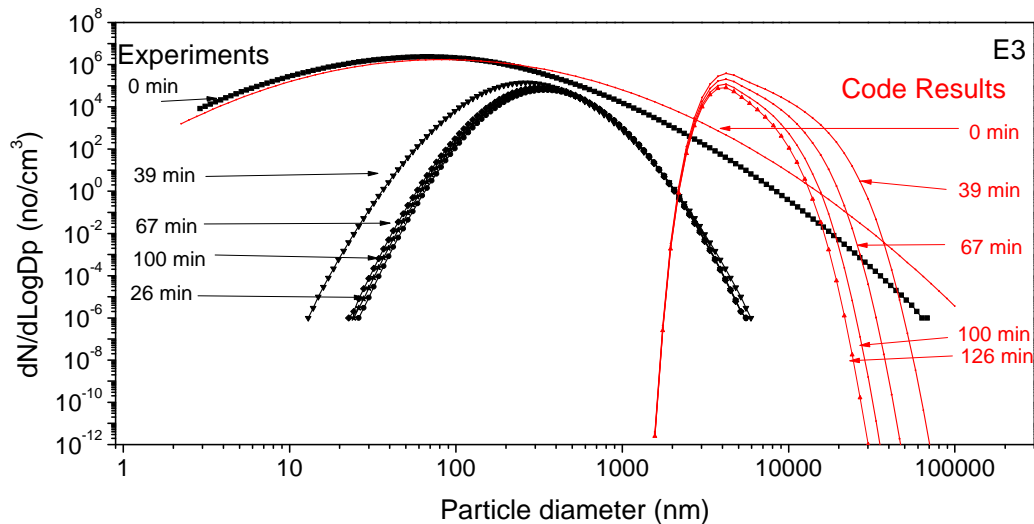


**Figure 5.12:** *Experimental and code predicted size distribution for E3*

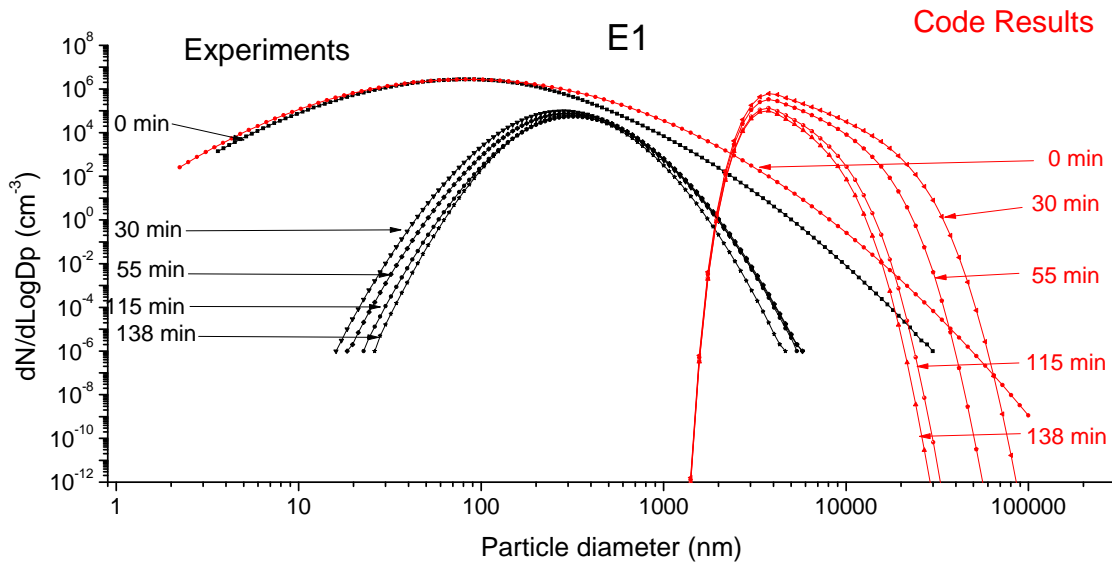


**Figure 5.12:** Experimental and code predicted size distribution for E1

This comparison resulted in discrepancies between code predictions and experiments. Two points can be noted at this juncture: 1) Code prediction for mean (or mode) size for both experiments (E1&E3) yielded similar results. 2) Code predicted mean size was significantly different from the experimentally observed mean size.

The prediction capability of NAUA MOD 5 code is limited in terms of condensational behavior due to use of Mason's equation where no provision for chemical behavior and consequent water uptake exists. For similar aerosol physical conditions, the change in aerosol size due to volumetric growth (condensation) should be same for different chemical species and this was observed while comparing code predictions for E1 and E3. At this moment, since the processed distributions were also observed to be similar hence the difference due to chemical interactions could not be seen in these figures. Such differences however were seen from CDP measurements where higher droplet concentration and LWC was observed for tin oxide aerosols.

Before looking at the comparison of the water content parameters predicted by the code with CDP measurements, inferences based on the above discussion can be drawn out as follows:

- 1) Code grows all aerosols instantly to the higher size (which was tested by checking the code predictions at very small times). Such high growth rates are expected due to use of Mason's equation. No aerosol remains un-activated and available steam is utilized in volumetric growth of all aerosols equally. In reality (as observed by experiments), either a fraction of aerosols remain un-activated (due to polydispersity constraint) or the volumetric growth can be less. This discrepancy arising due to steam distribution effect needs to be addressed. More insight into it can be developed by observing the changes in aerosol and droplet characteristics at all times.
- 2) In code predictions, the available steam was distributed among all aerosols. It means that the droplet concentration for such a case would be higher with lesser MVD. In reality, the same amount of steam will get distributed to lesser number of (activated) particles. In this condition, a higher volume equivalent diameter is expected. As will be seen, CDP measured volume equivalent diameter higher than code predicted average diameter. Steam-aerosol portioning is complex and code seems to be deviating from the realistic scenario.
- 3) CDP-measured average diameter was  $> 10 \mu\text{m}$ . For this diameter, even settling alone will result in a very fast decay rate particularly for the NATF chamber (of mid height 1.75 m). In these conditions, low concentration of droplet is expected if measurement starts even a few minutes after steam injection. Chamber volume (and surface area to volume ratio) can be a serious constraint for droplet measurements for carrying out steam experiments.

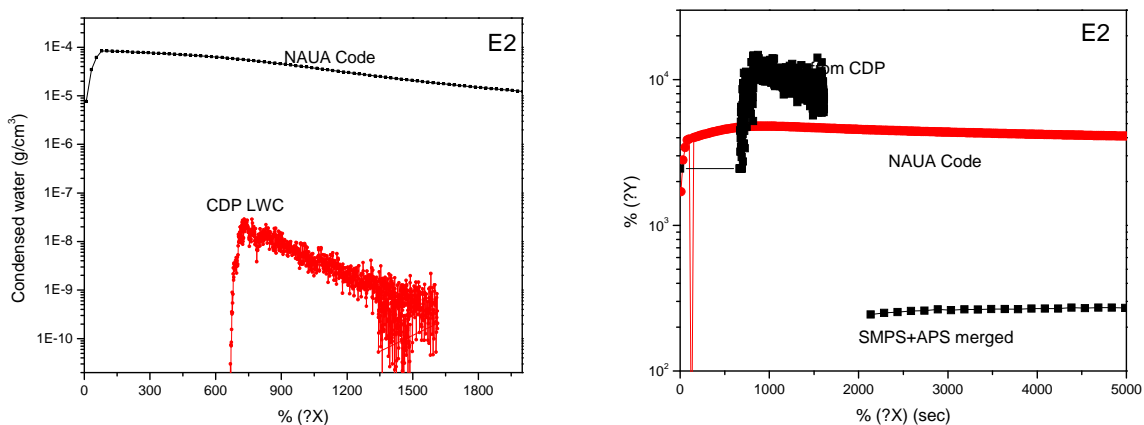


**Figure 5.13:** Experimental and code predicted LWC geometric mean diameter for E2

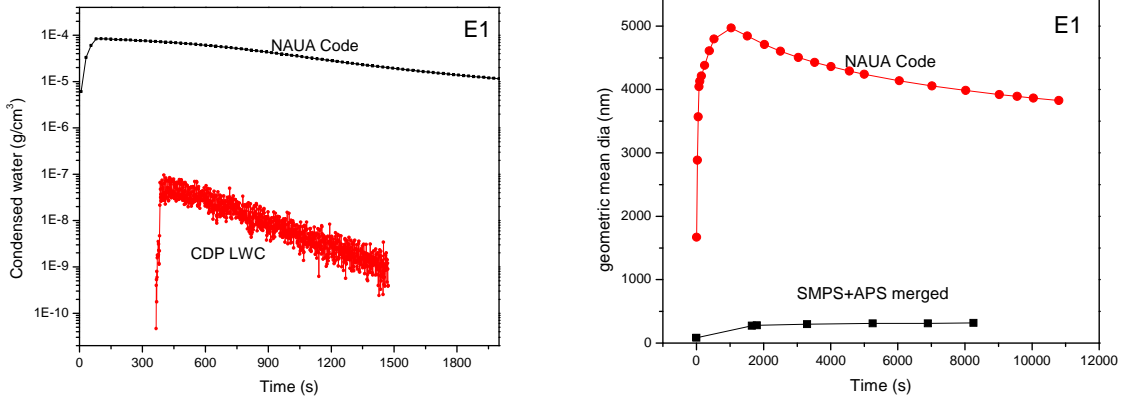


**Figure 5.14:** Experimental and code predicted LWC geometric mean diameter for E1

Figures 5.13 and 5.14 show comparison of code predicted average diameter with aerosol diameter (from merged SMPS and APS distribution) and droplet diameter (from CDP) for experiments E2 and E1. As explained and expected, code prediction was quite off compared to measured aerosol distributions and CDP measured diameter was also found to be larger. Expected higher MVD was clearly seen, however CDP measured LWC was also seen to be quite less than code predicted condensed water. It may be due to the constraint that CDP measures water content for particles/droplets greater than 3  $\mu\text{m}$  while code measures water content for one

Code predictions for Experiment (E6) for ambient conditions having significantly lesser number concentration of aerosols ( $\approx 8000 \text{ cm}^{-3}$ ) and higher mean size (145 nm) were also made and the size distribution evolution for this case is shown in Figure 5.15. As observed again even for this condition, code growth was unrealistic. It could be observed from this figure that even at 13 seconds for ambient conditions (having heterogeneity in terms of physical and chemical behaviour), code grew all aerosols to a significantly higher size.



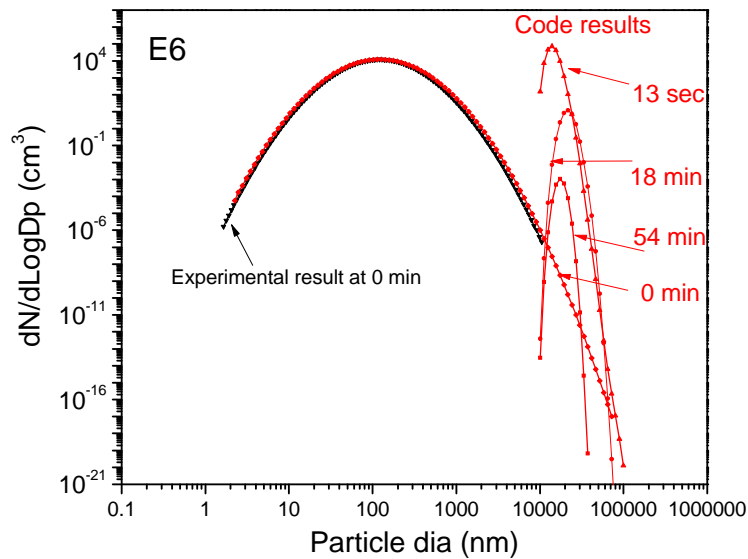


**Figure 5.15:** Code predictions of size distribution evolution for ambient conditions (E6)

All these experiments provided a conclusive insight for aerosol steam interactions in context of nuclear reactor accident research. The effect of chemistry on hygroscopic growth of metal oxide aerosols and significant differences with respect to evolved aerosol size distribution under steam condition is crucial towards understanding the microphysics of aerosol steam interactions.

## Chapter 6: Condensation Activation of CsI aerosols

Condensational behavior of CsI aerosols at various RH levels is important to study in context of reactor accident scenario. CsI is considered as most important volatile component which can be released from the reactor under accident conditions. Its hygroscopic response is also important to study and understand the differences vis-a-vis other atmospheric aerosol components (NaCl,  $(\text{NH}_4)_2\text{SO}_4$ , etc.), if any. Despite importance of knowing physico-chemical properties of CsI aerosols, detailed data on the properties of these aerosols (particularly hygroscopic response) are lacking. Very few studies have been performed mainly focusing on depositional behavior (such as Hidaka et al. 2000). For KI, Ephraim et al. 2007 have experimentally shown Deliquescence Relative Humidity (DRH) in range of 60-70 %. They have also reported growth factor curve (for dry size of 75-100 nm). As per our best knowledge, no such data exists for CsI aerosols. Although, the formation of CsI aerosols in case of high enthalpy reactor accidents is governed by evaporation-condensation process; preliminary indicative inferences can be attempted by exposing nebulized aerosols in controlled RH conditions. CCNC (used extensively for aerosol-cloud interaction studies) can be used for such a purpose. When coupled with SMPS, it can be used in polydispersed or size resolved (monodispersed) sampling mode for studying the hygroscopic response of aerosols. In polydispersed sampling, aerosols are passed simultaneously, through CPC, SMPS and CCN counter to measure the total number concentration of particles ( $N_{\text{CN}}$ ), size distribution and CCN concentration as a function of supersaturation, respectively. The CCN concentrations ( $\text{cm}^{-3}$ ) are then normalized by the total number of aerosol particles, yielding CCN activated fractions (CCN/CN ratio). Figure 6.1 shows schematic diagram for poly-disperse sampling.

In mono- dispersed sampling, the aerosols are first passed through the DMA to get size resolved particles, subsequently they are passed through CPC and CCN counter to measure total count and CCN, respectively (Figure 6.2). Most studies (to date) operate the DMA in “stepping mode” where the voltage applied to the DMA is increased stepwise to cover the entire size range of the DMA (Frank et al., 2006). During this study, the DMA is operated in “stepping mode”.

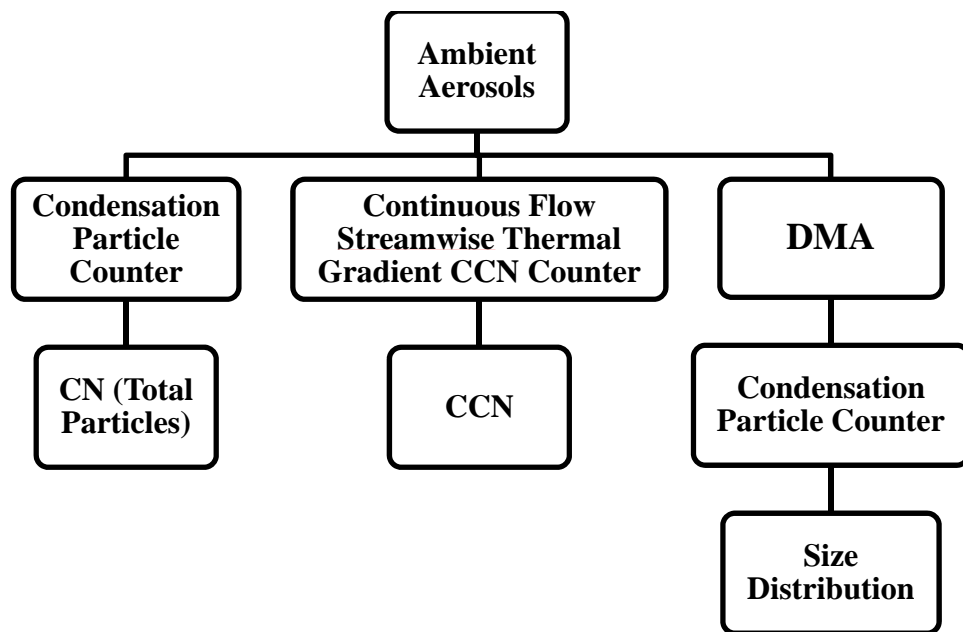


*Figure 6.1: Schematic showing the poly-disperse sampling using various instruments*

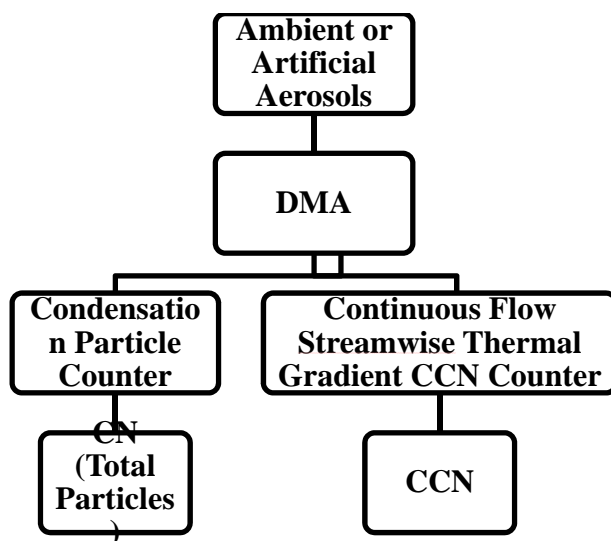


*Figure 6.2: Schematic showing the mono-disperse sampling using various instruments*

## 6.1 Experimental set-up

The experimental set up consists of TSI SMPS, continuous flow stream wise thermal-gradient CCN counter (DMT CCNc), CPC (TSI Model 3375), aerosol Generator (TSI model 3079) having adjustable flow rate from 1.0 to 4.2 Lmin<sup>-1</sup> and RH measuring device (Figure 6.3). Prior to all measurements, the ambient aerosols were dried down to RH (relative humidity) of 25 % by

passing through a denuder so that residual aerosol water does not affect the size of the particles; as this can result in a positive bias in CCN activity for very hygroscopic particles. The dried particles were then passed through a Krypton bipolar charger (TSI Model 3080) where they attain a known bipolar charge distribution. They subsequently enter the Differential Mobility Analyzer (DMA; TSI Model 3010) where they are classified on the basis of electrical mobility. The DMA is operated at a sample air flow rate of  $0.8 \text{ Lmin}^{-1}$ . The mono-disperse aerosol flow ( $0.8 \text{ Lmin}^{-1}$ ) was split into two parts: one to the CPC ( $0.3 \text{ Lmin}^{-1}$ ) and other to the DMT CCNc ( $0.5 \text{ Lmin}^{-1}$ ) to measure the number of particles, activated as CCN. HEPA filter was also used to maintain the sheath flow and the sample flow ( $0.8 \text{ Lmin}^{-1}$ ). For the size scan method, the CCN counter is set to a given and the CCN concentration is measured as a function of particle size (20 - 320 nm) corresponding to that supersaturation. During the experiment, the CCN counter was set at five different supersaturations (0.2, 0.4, 0.6, 0.8, 1.0 %) for a period of 2 minutes at each diameter.

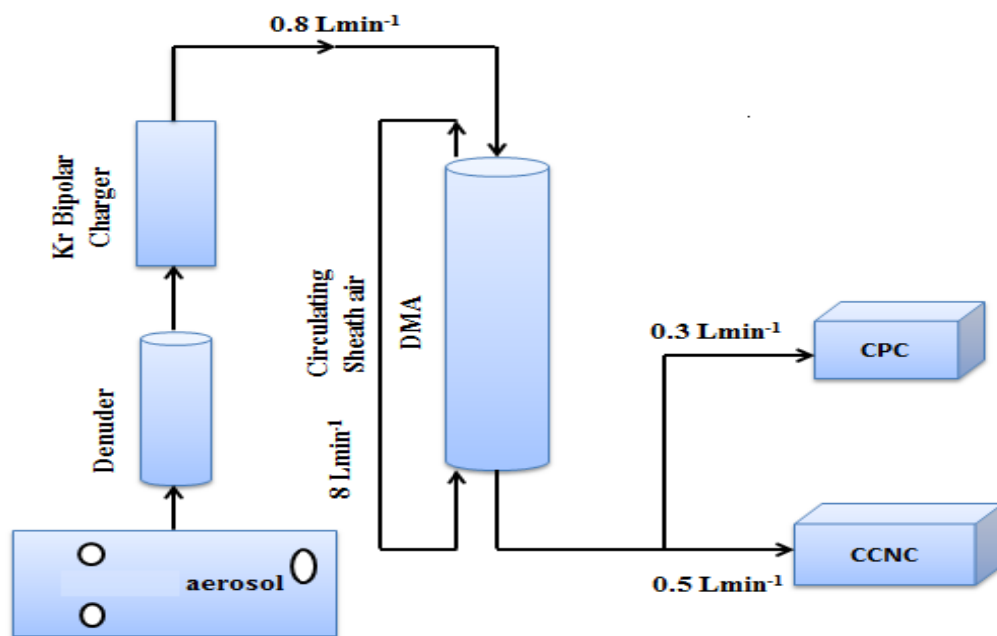


**Figure 6.3:** Sampling manifold for chamber experiments

A plexi-glass chamber of volume 39 liters was used for maintaining the steady state distributions for the mono-disperse aerosols (Figure 6.4). This chamber was equipped with a small fan to homogenize the aerosols and had provisions of four sampling ports. After removing background

aerosols from this chamber, CsI solution (concentration 0.3 % v/v) was nebulized and the dried CsI aerosols were filled in. The steady state number concentration and size distribution was recorded using CPC & SMPS.

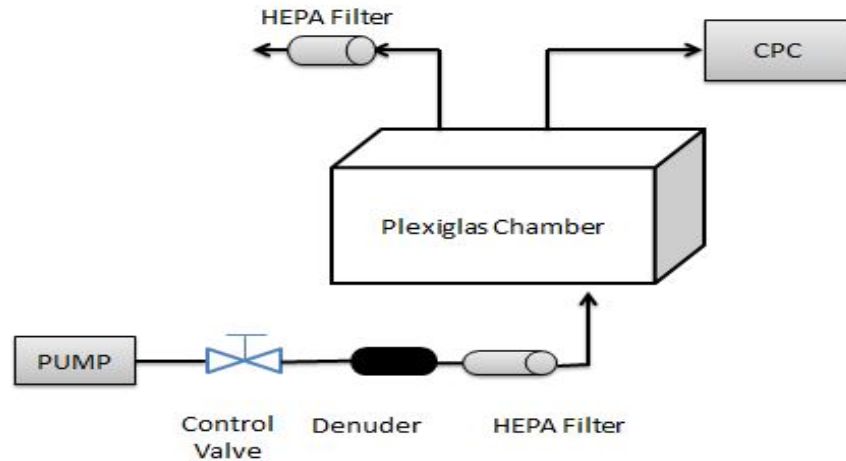


**Figure 6.4:** Schematic of aerosol generation and sampling in chamber

## 6.2 Results and Discussions

The time required to achieve the steady state concentration, determined using the flow balance of the connected instruments and the chamber volume comes out to be 30 minutes compared to the observed time of 38 minutes (by observing the particle concentration using CPC). Figure 6.5 shows the time series of CsI number concentration while Figure 6.6 represents an average aerosol size distribution sampled from the chamber.

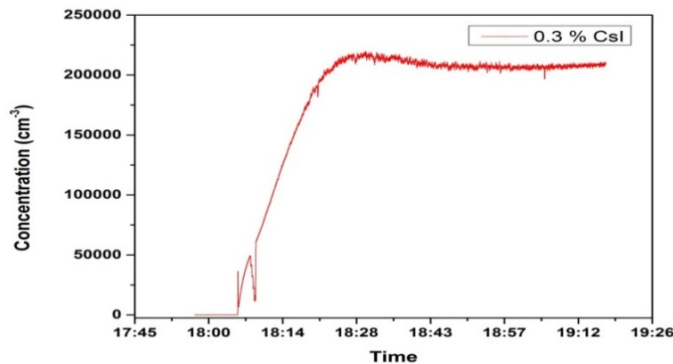


**Figure 6.5:** Time series of aerosol concentration inside the chamber (steady state)

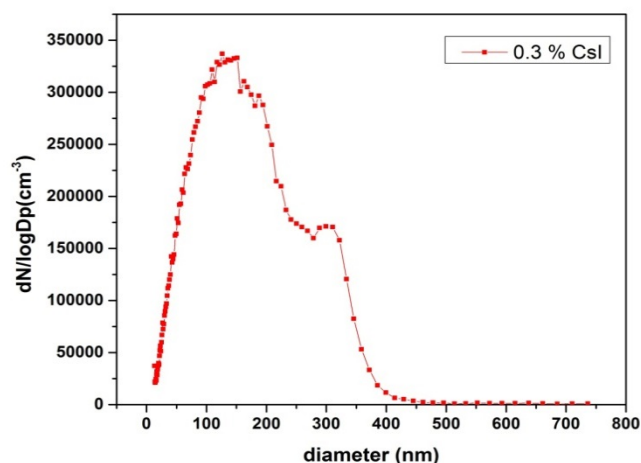


**Figure 6.6:** Average aerosol size distributions (0.014–0.68 $\mu$ m) for 0.3 % CsI solution

After achieving the steady state, the CCN counter is set to a given supersaturation (0.2, 0.4, 0.6, 0.8, 1.0 % ) and the CCN concentration is measured as a function of particle size (20 - 320 nm) corresponding to that supersaturation. Figure 6.7 shows the average size-resolved CCN/CN ratio at 0.2, 0.4, 0.6, 0.8 and 1 % supersaturation. In general, CCN/CN increases with increasing diameter. For lower supersaturation and smaller particles, e.g. 20-50 nm at 0.2 and 0.4% supersaturation, the activation ratios are close to 0. Size-resolved activation measurements show that most of the 300 nm particles are activated at the investigated supersaturation, while almost no particles of 20 nm are activated even at the highest supersaturation of 0.8 %. The activation fraction is calculated after applying multiple charge correction. The presence of multiply charged particles, which usually have higher activation ratio than the singly charged particle, induces a falsely higher measured activation ratio for singly charged diameters. The correction will reduce the activation ratio especially for the smaller particle sizes.

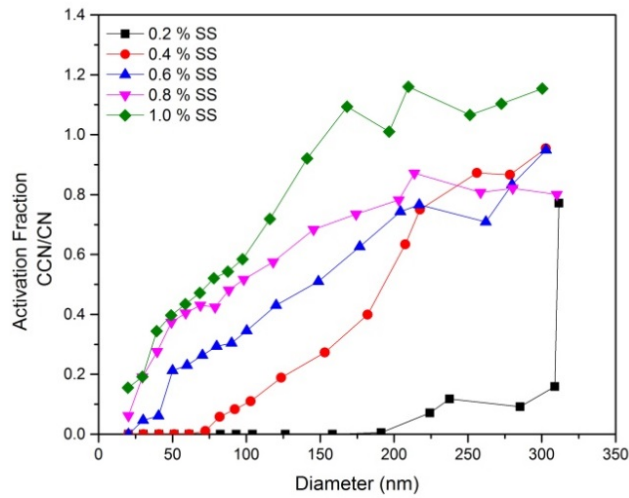


**Figure 6.7:** Activation fraction of CsI aerosols (for mono-disperse conditions)

The activation behavior at different supersaturation can also be seen as a function of changes in supersaturation conditions for three size groups (20-50 nm, 60-120 nm, 150-320 nm). Figure 6.8 (a, b, c) shows the difference of activation behavior for above selected size groups. As observed in Figure 6.8(a), low activation fraction was achieved for any supersaturation conditions while a significant activation fraction was seen for Figure 6.8 (c) above 0.4 % SS ratio. The intermediate size group showed transitional activation behavior.

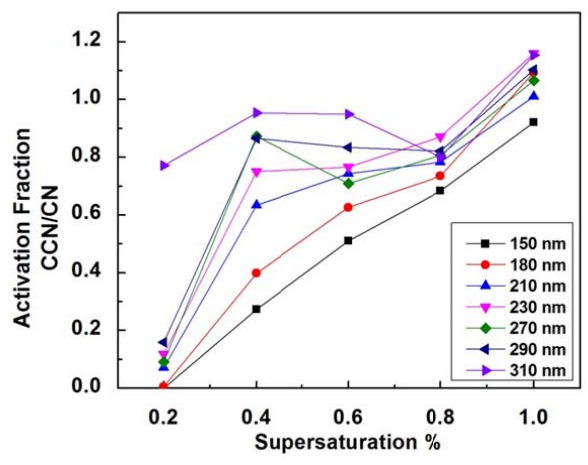
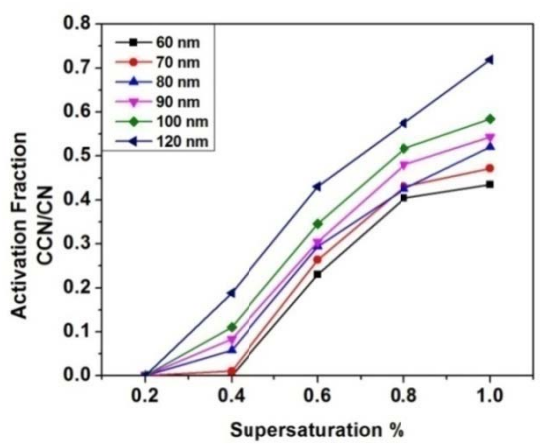
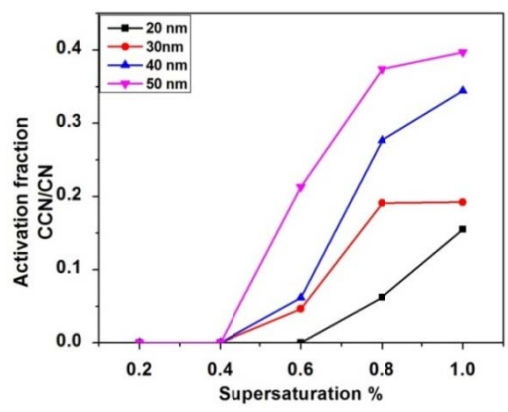


Figure 6.8 (a, b, c): Activation fraction of CsI aerosols (a) Lower size particles (20-50 nm) (b) middle size particles (60- 120 nm) (c) higher size particles (150-310 nm).



The diameter, at which 50% of the mono-disperse particles were activated i.e.  $D_{50}$ , is called critical dry particle diameter for CCN activation. It represents the diameter required for the particles with the given composition to be activated as CCN for a given supersaturation (Rose et al. 2008). Kohler theory was used to compute critical diameter for a given  $S_c$ , assuming the density and molar mass of CsI as  $4510 \text{ kgm}^{-3}$  and  $0.25981 \text{ kgmole}^{-1}$ , respectively.

$$S_c = \left[ \frac{256}{27} \left( \frac{M_w \sigma}{RT \rho_w} \right)^3 \left( \frac{M_s}{\rho_s} \right) \left( \frac{\rho_w}{M_w} \right) \frac{D_p^{-3}}{\varepsilon_s \nu_s} \right]^{1/2}$$

The effective van't Hoff factor  $\nu_s$  (which includes the effect of osmotic coefficient) was taken as 2 while  $\sigma$ , the surface tension of water was taken as  $0.07197 \text{ Jm}^{-2}$  for calculations. In above expression,  $\varepsilon_s$  is solute volume fraction, which is 1 if we consider the aerosols to be composed of a pure soluble compound. Table 4.6 shows the comparison of measured and theoretically predicted activation diameter for CsI aerosols.

**Table 6.1: Comparison of activation diameter for CsI aerosols (experiment and theory)**

Compound	Supersaturation %	Activation diameter (nm)	
		Measured	Theoretical
CsI	0.2	309	82
	0.4	200	51.5
	0.6	135	39.3
	0.8	90	32
	1.0	60	27

Some more experiments however are required to study CsI aerosol hygroscopic interactions before trying to explain the differences observed between theory and experiments.

## Chapter 7: Conclusions

- 1) A detailed inter-comparison study of GRIMM-SMPS (model no 5.403) available at Bhabha Atomic Research Center (BARC) and the TSI-SMPS (classifier 3080 with CPC 3775) available at the Indian Institute of Technology, Kanpur (IITK) was performed. For ambient conditions, the CPC results were within a factor of 1.05 while for high concentration comparisons, the CPC differences increased to a factor of 1.18. For ambient conditions, G-SMPS particle concentration results were 1.16–1.25 times higher than T-SMPS results. An excellent consistency was observed while comparing the mean size and geometric standard deviation from both the instruments. G-SMPS mean size was always approximately 10 % lower than T-SMPS mean size while GSD was seen to be almost similar. For laboratory generated aerosols, the difference of G-SMPS and T-SMPS results increased to 1.7–1.9 with almost similar inferences as ambient case for mean and GSD. These results have been used for harmonizing the measurements made with these SMPSs.
- 2) An experiment has been conducted to quantify the influence of hygroscopic growth of ambient particles on light absorption. GRIMM and TSI SMPSs have been used as a set-up to estimate dry and wet aerosol diameter (hygroscopic growth) at different RH conditions. The results have been used to model the chemical composition and optical properties of aerosols. The model has been verified by comparing the predictions with measured absorption and scattering coefficients over Kanpur region.
- 3) Six experiments (four with zinc oxide, one with tin oxide and one with ambient aerosols) have been performed in NATF for studying aerosol-steam interactions. The geometric mean diameter for zinc oxide aerosols (67 nm, 55 nm for two experiments) changed to approximately 300 nm (for both), respectively. For tin oxide aerosols, geometric mean diameter changed from 86 nm to 300 nm as an effect of steam action. All droplet phase parameters i.e. MVD, LWC and DNC were found to be higher for tin oxide aerosols in comparison to zinc oxide aerosols. Since, the physical parametric conditions (mean size before steam conditions) for zinc and tin oxide experiments were maintained same (using similar plasma torch conditions) hence the difference in droplet phase parameters could be attributed to their chemical properties mainly hygroscopicity. The results of these experiments have also been compared with NAUA MOD 5 predictions. Steam and

thermal conditions were almost similar for all experiments while aerosol parameters were taken as per actual measurements using the merged distributions. Other parameters were kept same during code runs. While comparison of gross number concentrations provided reasonable matching, size distribution comparisons resulted in discrepancies between code predictions and experiments. The limitations of NAUA code for steam phase predictions have been highlighted in this work.

- 4) Activation diameter of CsI aerosols have been measured at 5 different SS conditions. At 0.2 % SS, activation diameter was measured to be 309 nm which became lower for higher SS levels.

## References

- Aggarwal, S. G. and Kawamura, K. (2009). Determination of aerosol water content under near ambient humidity condition. Asian Aerosol Conference AAC09, Nov 24-27, 2009.
- Ankilov, A. et al. (2002). Intercomparison of number concentration measurements by various aerosol particle counters, *Atmos Res*, 62,177–207.
- Asbach, C. et al. (2009). Comparison of four mobility particle sizers with different time resolution for stationary exposure measurements, *J Nanopart Re*, 11, 1593–1609.
- Banerjee, S., Tripathi, S. N., Das,U., Ranjan, R., Jadhav, N., Singh, V.P., Jariwala, C., Sonkar, S., and Sarkar, S. (2012). Enhanced persistence of fog under illumination for carbon nanotube fog condensation nuclei, *Journal of Applied Physics*, 112, 2, AN:024901, doi: 10.1063/1.4736557.
- Beonio- Broccheieri, F. et al. (1988).Nuclear aerosol codes. *Nuclear Technology*, 81, 193-204.
- Bunz, H. et al. (1983). NAUA Mod4: A code for calculating aerosol behavior in LWR core melt accidents, code description and user's manual. Kfk 3554.
- Bunz, H. et al. (1983). NAUA Mod 5 and NAUA Mod 5-M: Two computer programs for calculating the behavior of aerosols in a LWR containment following a core melt accident. Kfk 4278.
- Bond, T. C., Habib, G. et al. (2006). Limitations in the enhancement of visible light absorption due to mixing state. *Journal of Geophysical Research-Atmospheres*, 111, D20.
- Ephraim, W. III et al. (2007). Phase Transitions and Surface Morphology of Surfactant-Coated Aerosol Particles. *J. Phys. Chem. A*, 111, 11013-11020.
- Frank, G. P., Dusek, U. and Andreae, M. O. (2006). Technical note: A method for measuring size resolved CCN in the atmosphere, *Atmos Chem. Phys. Discuss.*, 6, 4879–4895.
- Gieseke, J. A. et al. (1986). Source Term Code Package: A User's Guide. NUREG/CR-4587 (BMI-2138).

- Helsper, C., Horn, H. G., Schneider, F., Wehner, B., Wiedensohler, A. (2008). Intercomparison of five mobility particle size spectrometers for measuring atmospheric submicrometer aerosol particles, *Gefahrst Reinhalt Luft*, 68, 475–481.
- Hidaka, A. et al. (1995). Experimental and analytical study on the behavior of cesium iodide aerosol/vapor deposition onto inner surface of pipe wall under severe accident conditions. *J. Nucl. Sci. Technol*, 32, 10, 1047-1053.
- Hosemann, J. P. and Haschke, D. (1983). DEMONA: Aerosol Removal Experiments. EIR-Bericht Nr. 505.
- Jacobson, M. Z. (2001). Strong radiative heating due to the mixing state of black carbon in atmospheric aerosols. *Nature* 409, 6821, 695-697.
- Jariwala, C. G. (2009). An Observational and Laboratory study on the effects of cloud condensation nuclei and black carbon aerosols on fog persistence, M.Tech Thesis, IIT Kanpur.
- Joshi, M., Sapra, B. K. et al. (2012). Harmonisation of nanoparticle concentration measurements using GRIMM and TSI scanning mobility particle sizers. *Journal of Nanoparticle Research*, 14, 12, 1-14.
- Kaul, D. S., Gupta, T. et al. (2011). Secondary Organic Aerosol: A Comparison between Foggy and Nonfoggy Days. *Environmental Science & Technology*, 45, 17, 7307-7313.
- Koch, W., Pohlmann, G., Schwarz, K. (2008). A reference number concentration generator for ultrafine aerosols based on Brownian coagulation. *J Aerosol Sci*, 39, 150–155.
- Köhler, H. (1936). The nucleus in and the growth of hygroscopic droplets. *Trans. Faraday Soc.*, 32, 1152–1161.
- Kreidenweis, S. M., Petters, M. D. et al. (2008). Single-parameter estimates of aerosol water content. *Environmental Research Letters*, 3, 3.
- Kress, T. S. (1985). Review of areas that may require simultaneous coupled solution of the thermal hydraulic and fission product/aerosol behavior equations for source term determination.

Proceedings of the CSNI Specialist Meeting on Nuclear Aerosols in Reactor Safety, KfK 3800, CSNI95.

Lathem, T.L. and Nenes, A., (2011). Water Vapor Depletion in the DMT Continuous-Flow CCN Chamber: Effects on supersaturation and Droplet Growth. *Aerosol Sci. Technol.*, 45, 5.

Lui Peter, S. K., Deshler, Terry (2003). Causes of concentration differences between a scanning mobility particle sizer and a condensation particle counter. *Aerosol Sci Technol*, 37, 916–923.

Mason, B. J. (1971). *The physics of clouds*, Clarendon press.

Mayya, Y. S., Sapra, B. K. et al. (2005). Containment aerosol behavior simulation studies in the BARC Nuclear Aerosol Test Facility. Bhabha Atomic Research Centre BARC/2005/E/003.

Moosmuller, H., Chakrabarty, R. K. et al. (2009). Aerosol light absorption and its measurement: A review. *Journal of Quantitative Spectroscopy & Radiative Transfer*, 110, 11, 844-878.

Mulholland, G. W., Donnelly, M. K., Hagwood, C. R., Kukuck, S. R., Hackley, V. A., Pui, D. Y. H. (2006). Measurement of 100 nm and 60 nm particle standards by differential mobility analysis. *J Res NIST*, 11, 4, 257–312.

Nessler, R., Weingartner, E. et al. (2005). Effect of humidity on aerosol light absorption and its implications for extinction and the single scattering albedo illustrated for a site in the lower free troposphere. *Journal of Aerosol Science*, 36, 8, 958-972.

Patidar, V., Tripathi, S. N., Bharti, P. K., & Gupta, T. (2012). First Surface Measurement of Cloud Condensation Nuclei over Kanpur, IGP: Role of Long Range Transport. *Aerosol Science and Technology*, 46, 9, 973-982.

Roberts, G., and Nenes, A. (2005). A Continuous-Flow Streamwise Thermal-Gradient CCN Chamber for Atmospheric Measurements. *Aerosol Science and Technology*, 39, 206–221, doi:10.1080/027868290913988.

Sapra, B. K., Khan, A. et al. (2002). Aerosol behavior in BARC-Nuclear Aerosol Test Facility: objectives and experimental results. *IASTA bulletin*, 14, 1, 199-201.

Sapra, B. K., Mayya, Y. S. et al. (2008). Aerosol studies in a Nuclear Aerosol Test Facility under different turbulence conditions, *Nuclear Technology*, 163, 2, 228-244.

Schikarski, W. O., Schoeck, W. (1985). Proceedings of the CSNI specialist meeting on nuclear aerosols in reactor safety. KFK—3800 ; CSNI95.

Schlatter, J. (2006). Comparison of Grimm and TSI condensation particle counters. 10 ETH-Conference on Combustion Generated Particles Zurich, 21 to 23 August, ([http://www.metas.ch/metasweb/Fachbereiche/Partikel\\_und\\_Aerosole/Annexes/Dokumente\\_Nanopartikel/ETH2006GrimmTSI.pdf](http://www.metas.ch/metasweb/Fachbereiche/Partikel_und_Aerosole/Annexes/Dokumente_Nanopartikel/ETH2006GrimmTSI.pdf)).

Shamjad, P. M., Tripathi, S. N. et al. (2012). Comparison of Experimental and Modeled Absorption Enhancement by Black Carbon (BC) Cored Polydisperse Aerosols under Hygroscopic Conditions. *Environmental Science & Technology*, 46, 15, 8082-8089.

Sher, R. and Jokiniemi, J. K. (1993). NAUAHYGROS 1.0: A code for calculating the behavior of aerosols in nuclear plant containments following a sever accident. EPRI report, TR-102775.

Singh, V.P., Gupta, T., Tripathi, S.N., Jariwala, C. and Das, U. (2011). Experimental study of the effects of environmental and fog condensation nuclei parameters on the rate of fog formation and dissipation using a new laboratory scale fog generation facility, *Aerosol and Air Quality Research*, 11, 2, 140-154.

Sreekumar, K. P. et al. (1996). Plasma torch based aerosol generator. Bhabha Atomic Research Centre BARC/1996/E/007.

Srivastava, M., Tripathi, S. N., Dwivedi, A. K., Dalai, R., Bhattu, D., Bharti, P. K., Jaidevi, J., and Gupta, T. (2013). CCN Closure Results From Indian Continental Tropical Convergence Zone (CTCZ) Aircraft Experiment. *Atmospheric Research*, 132-133, 322-331.

Toon, O. B. and Ackerman, T. P. (1981). Algorithms for the calculation of scattering by stratified spheres. *Applied Optics*, 20, 20, 3657-3660.

Watson, J. G., Chow, J. C., Sodeman, D. A., Lowenthal, D. H., Chang, M. C. O., Park, K., Wang, X. (2011). Comparison of four scanning mobility particle sizers at the Fresno Supersite. *Particuology*. doi:10.1016/j.partic.2011.03.002.

Wiedensohler, A. et al. (2012). Particle mobility size spectrometers: harmonization of technical standards and data structure to facilitate high quality long-term observations of atmospheric particle number size distributions. *Atmos Meas Tech*, 5, 657-685.



## **Acknowledgment**

**The PI gratefully acknowledges the funding support under the BRNS program of DAE. We thank Dr. Y. S. Mayya for his overall guidance to the project. The PI also places on record his sincere appreciation for Sri H. S. Kushwaha for his continuous encouragement and support.**



## **Project Review Committee**

### **Chairman & Members, R&E, NRFCC, BRNS**

1. Shri H.S. Kushwaha, Raja Ramanna Fellow, DAE - Chairman
2. Shri P.K. Wattal, Head, PSSD, BARC - Member
3. Dr. Om Pal Singh, Visiting Faculty, IIT-Kanpur (Ex-AERB) - Member
4. Shri V.D. Puranik, Head, EAD, BARC - Member
5. Dr. Y.S. Mayya, Head, RP&AD, BARC - Member
6. Dr. A.G. Hegde, Ex-Head, ESS, HPD, BARC - Member
7. Dr. P.V. Ramesh Babu, Reg. Dir. (SC), AMD, Hyderabad - Member
8. Dr. P.C. Verma, Ex-HPD, BARC - Member
9. Dr. D. Roy, Programme Officer, BRNS - Member
10. Dr. R.M. Tripathi, Head, RPS(NF), EAD, BARC - Member Secretary